POLITECNICO DI TORINO

Dipartimento di Ingegneria Meccanica e Aerospaziale

Corso di Laurea Magistrale
in Ingegneria Aerospaziale

Tesi di Laurea Magistrale

Preliminary study for the design of a Ballbot

Relatore

Prof. Mauro Stefano

Correlatore

Prof. Pastorelli Stefano Paolo

Ing. Melchiorre Matteo

Candidato

Juan Pablo Chevalie

Settembre 2018

Abstract

The aim of this thesis is the study and modeling of an innovative concept of mobile robot called Ballbot, this robot is designed to be dynamically stable on a single ball, due to its omnidirectionality this robot presents an astounding mobility which makes it very interesting to be applied in human environments.

Firstly, in order to understand the dynamical behavior of this robot, a physical model was developed following a top-down approach, starting with a simplified model of a two-dimensional decoupled system. Later this model was improved by the introduction of physical phenomena originally idealized, which include the friction force with nonlinear behavior and the presence of a sloped surface. Finally, a linearized three-dimensional model was introduced in order to analyze the coupling terms between cartesian planes.

Due to the natural instability of the Ballbot a sophisticated control is required, to achieve this goal an optimal control theory was used, implementing an LQR (linear–quadratic regulator) controller. The controller was designed to compute the proper motor torque aiming to meet the system stability and achieve a velocity tracking.

Once the control system was designed, the influence of the fundamental parameters as height, mass and center of gravity, were analyzed. The choice of those parameters will determine the response characteristics of the robot in terms of maximum tilt angle, performance and agility.

Finally, the work ends with several simulations with different input requirements which may require some future applications of the Ballbot, in each case the response was studied in order to optimize the control system.

Index

List of Figures

List of Tables

Acknowledgements

I would first like to thank my thesis advisors, Prof. Stefano Mauro and Prof. Stefano Paolo Pastorelli for their guidance, assistant and support during the project.

I would also like to acknowledge to Matteo Melchiorre as co-advisor of this thesis, I am gratefully indebted to him for his very valuable remarks on this thesis.

Finally, I must express my profound gratitude to my parents and to my friends for providing me with constant support and continuous encouragement throughout my years of study. This accomplishment would not have been possible without them. Thank you.

Juan Pablo Chevalie

Chapter 1 - Introduction

1.1 Motivation

Historically, mobile robots have been designed to be statically stable, which results in the robot not needing to expend energy while standing still. This is typically achieved through the use of three or more wheels on a base. These statically-stable mobile robots have a wide base for a large polygon of support, and a lot of dead weight in the base to lower the center of gravity. The wide base makes it difficult for statically-stable mobile robots to navigate cluttered human environments. Moreover, these robots have several other limitations that make them poorly suited to a constantly changing human environment. They can neither roll in any direction, nor can they turn in place [1].

In this context arises the need to develop a new concept of mobility, with a design that gives omnidirectionality to the vehicle, this means a configuration capable of moving in any direction without a previous need to reach a specific orientation.

1.2 The Ballbot concept

A Ballbot is a mobile robot able to stay stable and move on a single spherical wheel (i.e., a ball).

The Ballbot obtains the property of omnidirectionality due to its single contact point with the ground, that makes it agile, maneuverable and able to operate in complicated environments.

Whereas the main feature of this robot is to have a single contact point with the ground (Figure 1.1(a)), that generate a natural instability as that of an inverted pendulum. Thus, keep the equilibrium point requires an active control system. The

drive system works with an inverse computer mouse mechanism principle (Figure 1.1 (b)) to provide torque to the ball, while the body has no direct actuation.

The motion principle of the Ballbot is similar to the one of the Segway i.e. controlling the position of the center of mass (CM) of the system. When the CM moves forward, the motors accelerate towards the same direction in order to maintain the balance of the system. The more the CM shifts from the balancing point, the larger the acceleration in that direction [2].

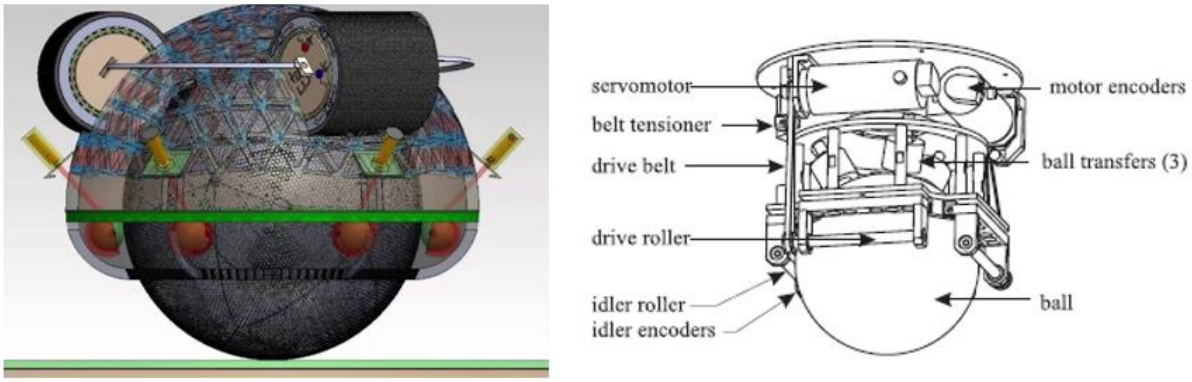

Figure 1.1: At the left (a) Ballbot side view. At the right (b) mouse-ball drive mechanism used by CMU Ballbot

1.3 Practical applications

The Ballbot concept has several possible practical applications, its design is adaptable to mass and height variations, which makes it an ideal nominee for a human mobile robot that would work as an omnidirectional Segway, taking as input, the movements of the driver or tracking an input device like a control column (Figure 1.2 (a)).

Another possible application is the use as an assistance robot, with a host of practical fields such as office jobs, home assistance, medical assistance and so on (Figure 1.2 (b)). Notably, a Ballbot device works in relatively smooth and even surfaces, which limits its application.

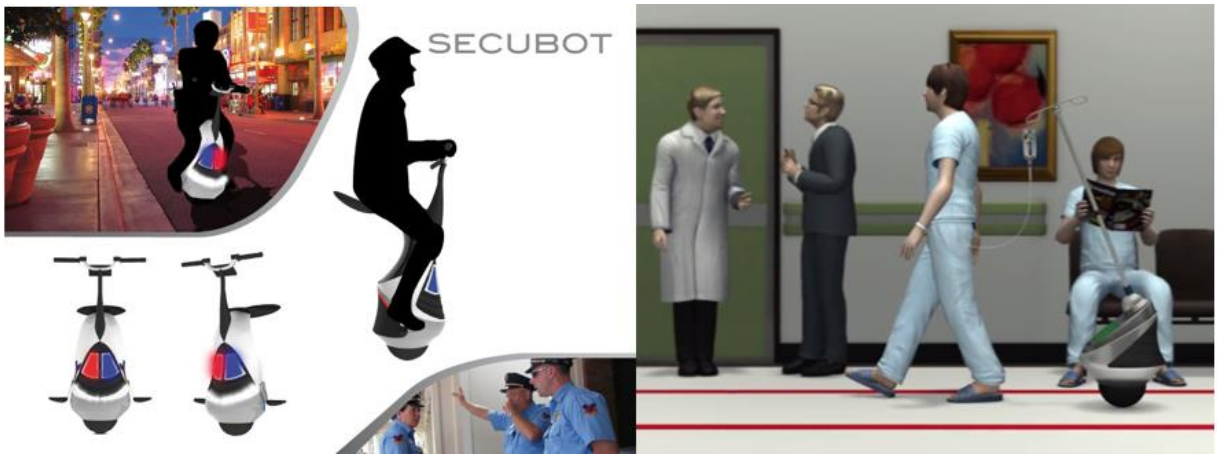

Figure 1.2 Possible applications of the Ballbot, at the left (a) human mobile robot. At the right (b) medical assistance. both proposed by [3]

In this thesis we focus on designing a Ballbot for large payloads (50 kg or more). Although this work does not focus on a specific application the research done is applicable for a human mobile robot or an unmanned device.

Chapter 2 - State of the art

In this chapter, we will make a brief historical review about the development of robots based on inverse pendulum principle, starting with the one that maybe is the precursor of this device, the Segway. Then, by entering the specific field of the Ballbot we will make a brief description about the most notable devices and prototypes developed in the academic field, among them, the **CMU Ballbot** (The first successful Ballbot), developed by Prof. Ralph Hollis, the **Rezero** developed at ETH Zurich and finally an interesting concept of human-readable Ballbot named **B. B. Rider** developed at the university of Tokyo.

2.1 The Segway

One of the first devices that use the inverted pendulum principle is the **Segway PT (personal transporter) a** two-wheeled, human readable device developed by Dean Kamen. The working principle of a Segway is based on controlling the position of the center of mass (CM) of the system. The user's orientation is observed about 100 times per second using gyroscopes and tilt sensors within the vehicle.

Figure 2.1 Segway operating principle [2]

To move the Segway forward or backward, the rider simply leans slightly forward or backward respectively, Figure 2.1. When the CM moves forward, the motors of the Segway accelerate towards the same direction in order to maintain the balance of the

system. The more the CM shifts from the balancing point, the larger the acceleration in that direction. A manual turning mechanism on the control bar is used to steer the vehicle [2].

2.2 CMU Ballbot

The was first Ballbot built in 2005 [4] by Prof. Ralph Hollis of the Robotics Institute at Carnegie Mellon University (CMU). The goal of Prof. Hollis and his team have developed a new type of mobile robot (Figure 2.2) that is the height, width, and weight of a person, having a high center of gravity, that balances dynamically on a single spherical wheel. this robot must be slender enough to easily maneuver in cluttered, peopled environments, this research group also developed group a robust control system able to withstand large disturbances, and handle crashes with objects [5]. This device presents interesting applications in human-robot collaboration.

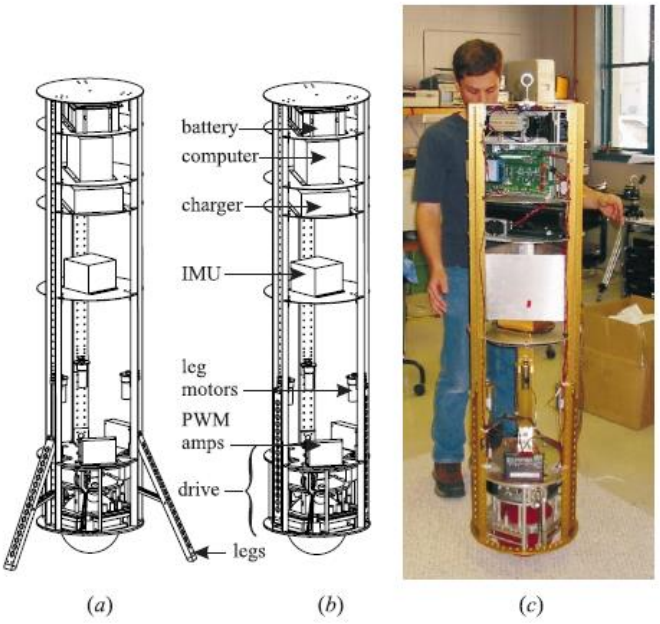

Figure 2.2: CMU Ballbot: (a) with three legs deployed, (b) with legs retracted into body, (c) balancing and station keeping [4]

2.3 Rezero

This Ballbot was developed in 2010 by a research group at ETH Zurich, [6] this device is one of the most sophisticated in the field. Not only is it able to stabilize and move in a sphere but also interacts with the environment, by means of a laser distance sensor. The sensor it is able to set up a distance with a person and follow it. Compared with other prototypes, Rezero reach fast responses and agile motions that can be achieved using Ballbots.

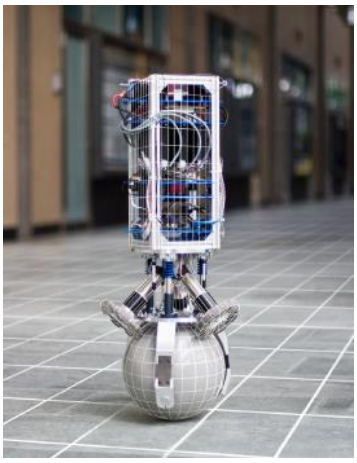

Figure 2.3: Rezero Ballbot

2.4 BB Rider

An interesting case to analyze is that of the BB rider, a human-readable Ballbot developed at the same time as the CMU Ballbot (2005) by a group of researchers led by Yoshihiko Nakamura from the University of Tokyo [7]. They presented this human mobility device that balances on a basketball, Nakamura and his group proposed an operating principle similar to that of the Segway, this means, who rides on the vehicle, can moves to all directions by shifting one's the center of mass.

However, the Ballbot did not reach a consistently stabilization and no extra labor was presented.

Figure 2.1 ″B. B. Rider″ Ballbot

Chapter 3 - Preliminary Design

In order to perform a preliminary study of the operation and performance of this device, it is necessary to define a preliminary design, specify geometric parameters and the macrostructure of the Ballbot. In order that, some existing devices will be studied, and a new design based on requirements needed will be proposed.

3.1 Main requirements

3.1.1 Performance and functionality

This section presents the main requirements that the prototype of the Ballbot must meet, in future calculations the other requirements must be adapted to meet these ones.

- The Ballbot must be able to stabilize and transport a large payload (50 kg or more)
- The Ballbot must maintain stable against disturbances of 5% of the maximum load.
- The Ballbot shall follow a velocity input given by the user.

3.1.2 Control requirements

In chapter 4 the controller will be designed to meet these requirements:

- Stable system i.e. all the closed loop poles should have a respective negative real part.
- Overshoot in body pitch angle response to a step input should be less than 10º.
- The control system must decrease frequencies above 80 Hz for at least 70% in order to guarantee the correct data acquisition by the IMU.
- The settling time of the inverse step response of the pitch body angle should be between 5 and 6 seconds in case of position keeping.

- Torque saturation should be minimized.

3.2 Drive mechanism

The motion principle of the Ballbot requires that the ball can be moved in any direction. This may be achieved implementing actuated wheels, the disposition of these actuated wheels it can be realized by several possible arrangements.

The table 3.1 shows a tradeoff analysis with the different types of arrangements used in functional prototypes at this moment and summarized in [8]. In order to perform a qualitative assessment, it is necessary to define figures of merit, among which, is highlighted:

- Construction (/10): How easily will be the construction or prototyping.
- Controllability (/10): How directly the action on the motor system is related to the Ballbot motion.
- Encumbrance (/10) understands, how many parts and transmission elements must be used and its influence on the total weight of the device.
- Friction (/10): it is understood as the spent energy, necessary to overcome friction, directly related to the number of pieces in contact with the sphere.

Assigning a relative value to each of these figures of merit, it was concluded that the best drive mechanism is use three omniwheels over ball center (Table 3.1)

Table 3.1 Trade off Matrix: Drive Mechanism

Concept	Controllability	Construction	Encumbrance	Friction	Final score
Four friction wheels at ball center Figure 3.1 (a)	9	5	3	3	20
Two omniwheels at ball center and one omniwheel for yaw movement. Figure 3.1 (b)	7	6	5	8	26
Four omniwheels over ball center Figure 3.1 (c)	6	7	6	6	25
Three omniwheels over ball center Figure 3.1 (d)	5	9	8	8	30

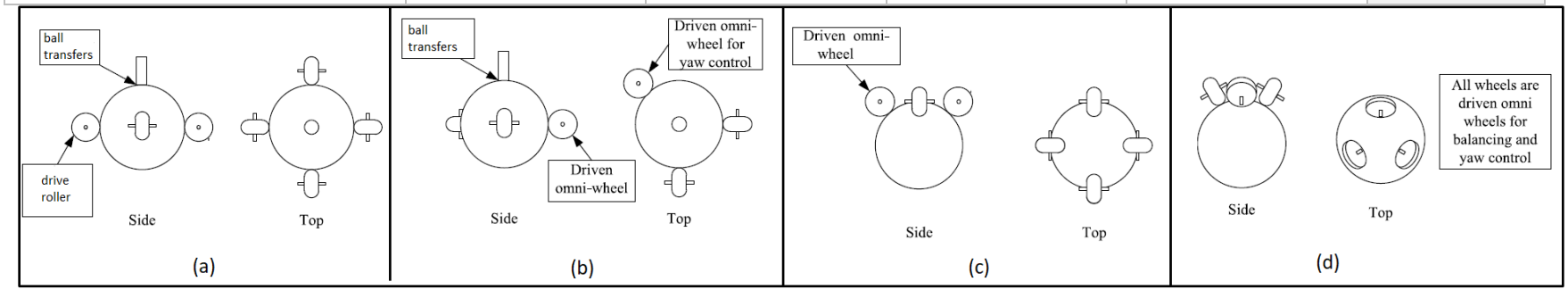

Figure 3.1 : (a) Four friction wheels at ball center. (b) Two omniwheels at ball center and one omniwheel for yaw control. (c) Four omniwheels over ball center. (d) Three omniwheels over ball center. Images by [8]

3.2 Geometric parameters

In order to obtain a functional mathematical model and perform future simulations, it is necessary to define certain geometric parameters as shown in table 3.2.

In chapter 6 we will see how these parameters influence the dynamics of the Ballbot.

Table 3.2 Geometric parameters of the preliminary design

Parameter	Symbol	Value
Distance between CM and ball center	l	$0.6\ [m]$
Ball radius	R_s	$0.16\ [m]$
Ball mass	M_s	$2.5\ [kg]$
Ball inertia	J_s	$0.016[kg.m^2]$
Pitch moment of inertia about CM	J_ψ	$12.48\ [kg.m^2]$
Roll moment of inertia about CM	J_φ	$12.48\ [kg.m^2]$
Body mass	M_b	$50\ [kg]$

Chapter 4 - Model Design

4.1 Planar system model

This section describes the mathematical model according to the work carried out by Yorihisa Yamamoto [9]. His methodology will be followed performing new assumptions and different simplifications according to our model described in chapter 3.

4.1.1 Description of two-dimensional model

As a first step we can take the Ballbot model and consider it as an inverted spherical pendulum without considering the omnidirectional wheels as an initial approach (Figure 3.1) thus the final system involves two rigid bodies, called the sphere and the body. In order to take the three-dimensional problem and reduce it to a two-dimensional system we must make the following assumptions:

- The motion in the pitch and roll plane (XZ and YZ respectively) are decoupled.
- The device present revolution symmetry therefore the equations for both planes are identical.

We also make the following simplifying hypothesis.

- There is no slip between the sphere and the ground.
- As a first approximation we consider rolling friction as negligible.

We take the XZ plane and present the model in a system of cartesian axes where we introduce the coordinates and main parameters involved. At this point we can notice that the system has two degrees of freedom, the body pitch angle(ψ) and the sphere rotation angle (θ).

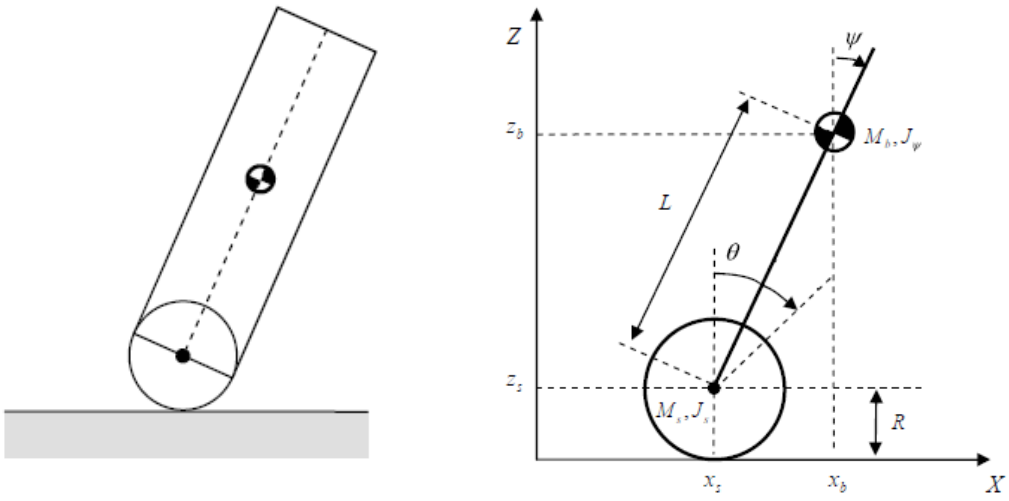

Figure 4.1: inverted spherical pendulum with coordinate system

We propose to find a relationship between the torque applied to the sphere and the response of the variables ψ and θ.

4.1.2 Kinetic relationships

Based on the coordinate system of the figure 3.1, Assuming that $\theta = 0$ at $t = 0$ it is possible to express the kinematic relationships of the system as:

$(x_s, z_s) = (R_s\theta, z_s)$

$(\dot{x}_s, \dot{z}_s) = (R_s\dot{\theta}, 0)$

$(x_b, z_b) = (x_s + L\sin\psi\,, z_s + L\cos\psi)$

$(\dot{x}_b, \dot{z}_b) = (R_s\dot{\theta} + L\,\dot{\psi}\cos\psi\,, -L\,\dot{\psi}\sin\psi)$

4.1.3 Dynamics equations

At this point it's possible derive motion equations with the method of Lagrange for this it is necessary to define, a mathematical function called the Lagrangian, which summarizes the dynamics of the entire system, this function is expressed as follows:

$$L = T_1 + T_2 - U$$

Where:

- T_1: Translational kinetic energy
- T_2: Rotational kinetic energy
- U: Potential energy

The ranslational kinetic energy is expressed as the as the sum of the energy of the body and the energy of the sphere

$$T_1 = \frac{1}{2}M_s\left(\dot{x_s}^2 + \dot{z_s}^2\right) + \frac{1}{2}M_b\left(\dot{x_b}^2 + \dot{z_b}^2\right)$$

Introducing θ e ψ

$$T_1 = \frac{1}{2}M_s\left(R_s\dot{\theta}\right)^2 + \frac{1}{2}M_b\left(\left(R_s\dot{\theta} + L\,\dot{\psi}\cos\psi\right)^2 + \left(L\,\dot{\psi}\sin\psi\right)^2\right)$$

Otherwise the expression of the rotational kinetic energy is given by:

$$T_2 = \frac{1}{2}J_s\dot{\theta}^2 + \frac{1}{2}J_\psi\dot{\psi}^2$$

and finally, the potential energy is expressed like:

$$U = M_s g z_s + M_b g z_b$$

considering that $z_b = z_s + L\cos\psi$ it is possible to manipulate the last equation to arrive at:

$$U = (M_s + M_b)g z_s + M_b g L\cos\psi$$

Taking theta (θ) and psi (ψ) like system degrees of freedom it is possible to obtain the equations of motions using the Lagrange's equations of the second kind.

$$\frac{d}{dt}\left(\frac{\partial L}{\partial\dot{\theta}}\right) - \frac{\partial L}{\partial\theta} = F_\theta$$

$$\frac{d}{dt}\left(\frac{\partial L}{\partial\dot{\psi}}\right) - \frac{\partial L}{\partial\psi} = F_\psi$$

Developing this last expression (see appendix A) we arrive at:

$$\left[(M_b + M_s)R_s^2 + J_s\right]\ddot{\theta} + [M_b L R_s\cos\psi]\ddot{\psi} - M_b L R_s\dot{\psi}^2\sin\psi = F_\theta \qquad (4.1)$$

$$[M_b L R_s\cos\psi]\ddot{\theta} + \left[M_b L^2 + J_\psi\right]\ddot{\psi} - M_b g L\sin\psi = F_\psi \qquad (4.2)$$

4.1.4 Linearization of the model

In order to obtain a state space representation to apply modern control theory techniques the equations 4.1 and 4.2 must be linearized. To do this, was chosen the

equilibrium point ($\psi = 0$) as a point of linearization, it means: $\sin\psi \to \psi$, $\cos\psi \to 1$ and neglecting the second order term $\dot{\psi}^2 = 0$. We arrive to the expression:

$$\left[(M_b + M_s){R_s}^2 + J_s\right]\ddot{\theta} + [M_b L R_s]\ddot{\psi} = F_\theta \quad (4.3)$$

$$[M_b L R_s]\ddot{\theta} + \left[M_b L^2 + J_\psi\right]\ddot{\psi} - M_b g L\psi = F_\psi \quad (4.4)$$

That can be reformulated as

$$E\begin{bmatrix}\ddot{\theta}\\ \ddot{\psi}\end{bmatrix} + F\begin{bmatrix}\dot{\theta}\\ \dot{\psi}\end{bmatrix} + G\begin{bmatrix}\theta\\ \psi\end{bmatrix} = \begin{bmatrix}F_\theta\\ F_\psi\end{bmatrix}$$

Where

$$E = \begin{bmatrix}(M_b + M_s){R_s}^2 + J_s & M_b L R_s\\ M_b L R_s & M_b L^2 + J_\psi\end{bmatrix}$$

$$F = [\bar{0}]$$

$$G = \begin{bmatrix}0 & 0\\ 0 & -M_b g L\end{bmatrix}$$

4.1.5 State Space Formulation

So far, we have arrived to a linear differential equation system with constant coefficients that can be written in **state-space representation** where the state variables are whose values evolve through time:

$$\bar{x} = [\theta, \psi, \dot{\theta}, \dot{\psi}]$$

Besides, the input or control will be the motor torque applied to the sphere

$$u = F_\theta$$

Thus, we can derive state equations from equations 4.3 and 4.4

$$\dot{x} = A\bar{x} + Bu$$

Where:

$$A = \begin{bmatrix}0 & 0 & 1 & 0\\ 0 & 0 & 0 & 1\\ 0 & A(3,2) & A(3,3) & A(3,4)\\ 0 & A(4,2) & A(4,3) & A(4,4)\end{bmatrix} \qquad B = \begin{bmatrix}0\\ 0\\ B(3)\\ B(4)\end{bmatrix}$$

$A(3,2) = -M_b gL\, E(1,2)/\det(E)$ $B(3)=[\, E(2,2) + E(1,2)]/\det(E)$

$A(4,2) = M_b gL\, E(1,1)/\det(E)$ $B(4)=[\, E(1,1) + E(1,2)]/\det(E)$

$A(3,3) = -[\, E(2,2) + E(1,2)]/\det(E)$ $A(3,4)=[\, E(2,2) + E(1,2)]/\det(E)$

$A(4,3) = [\, E(1,2) + E(1,1)]/\det(E)$ $A(4,4) = [\, E(1,1) + E(1,2)]/\det(E)$

4.2 Friction modeling

The friction phenomenon is a complex, nonlinear problem, involved in many areas of engineering. Modeling of friction is very important in pre-design phase. The correct representation of this phenomenon will be directly related to the veracity of the simulation.

Delving into the Ballbot problem, the main acting friction force is the rolling resistance.

4.2.1 Rolling resistance

Considering the sphere of the Ballbot resting on the ground and subjected to a load F_N, due to the weight of the entire device. Since the ball material is elastic, the contact between the body and the ground becomes a surface. In order to counteract the action of external forces i.e. the weight, arises a pressure distribution on this surface. In the absence of movement, the pressure distribution is symmetrical, thus, the resulting is collinear with the force F_N, therefore there is no resistant moment (Figure 4.2 (a)).

In rolling condition, it is verified that the resulting pressure distribution is asymmetrical and is shifted in the direction of motion, thus the reaction force no longer passes through the center of the ball instead is moved a distance u, called rolling resistance parameter. This creates a moment that tends to stand against the rolling torque M_v (Figure 4.2(b)).

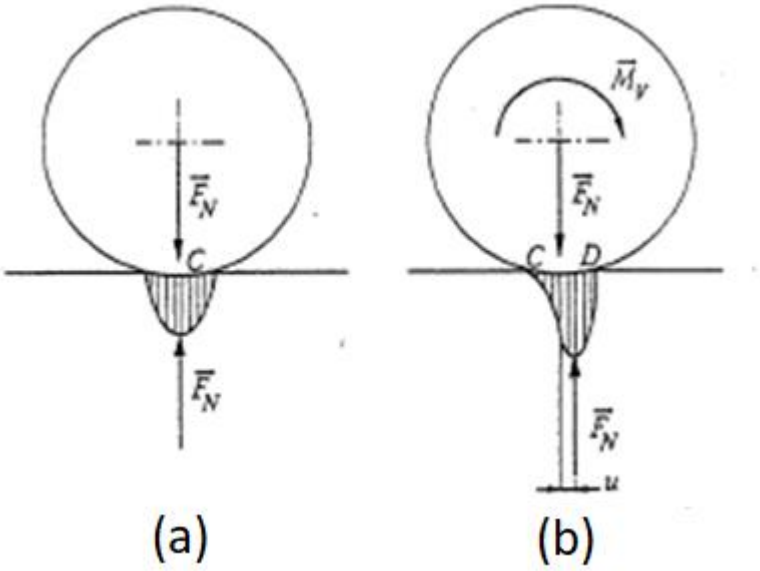

Figure 4.2 (a) pressure distribution reaction on a static condition (b) pressure distribution reaction on a rolling condition [10].

As regards the rolling resistance evaluation, the rolling friction coefficient often replaces the rolling friction parameter u. This non-dimensional coefficient, is defined as following:

$$f_v = \frac{u}{r}$$

Concerning that the rolling friction coefficient grows with the increase of the rolling speed, as demonstrated in the following law:

$$f_v = f_{v0} + f_v \omega^2 \qquad (4.5)$$

In conclusion, for have a correct representation in the model, we must add a resistance moment given by:

$$M_R = F_N . R_s . f_v$$

4.2.2 Numerical Model

To model the behavior of the resistant moment it is necessary to employ a simulation routine able to handle the dynamic behavior of the friction, this means that the software should be able to distinguish between the static condition and the slipping and to compute the eventual stop of the previously running rolling ball.

Several systems have been conceived, many of them based on the Coulomb friction model and with the use of discontinuous arrangement in this paper we will use the model proposed by L. Borello [11].

4.2.3 Borello friction model and related algorithm

In [11] the authors conceived an algorithm according to the aforesaid physical friction model with a layout not so different from the Karnopp's structure [12]; as the authors claims "both of them are divided in two alternative procedures related to the sticking or slipping condition. In sticking conditions, the friction force/torque is considered equal to the sum of the active forces/torques and opposing it, but its absolute value must be not greater than its limit represented by the static value of friction (FS)".

The mathematical model can be expressed as:

$$C_{friction} = \begin{cases} -C_M & if\ \ \omega = 0\ \wedge\ |C_M| \leq C_S \\ -sgn(C_M)C_S & if\ \ \omega = 0\ \ \wedge\ \ |C_M| > C_S \\ -sgn(C_M)C_D & se\ \ \omega \neq 0 \end{cases}$$

Where $C_{friction}$ represents the computed friction Moment, C_S is the value of the friction torque under static conditions and, C_D is the frictional force under dynamic conditions, function of the velocity and C_M denotes the active torque applied to the system

The authors' Simulink algorithm implements the aforesaid breakaway detection by means of a switch block that, as a function of instantaneous value of *DXJ* (velocity parameter), selects between sticking and slipping condition (by means of a hit crossing block) and, so, gives in output the proper value of static or dynamic friction

force *FF* (block A in Figure 4.3). In slipping conditions, the friction force/torque is the sum of a viscous and a constant term, opposing the motion; the viscous term is computed, by the coefficient *CJ*, within *Act_Th* in statement 1, while the constant one is equal to the dynamic value of friction *FD*, according to the statement 2. The result is, by the statement 4, an acceleration value *D2XJ* proportional to the difference between *Act_Th* and *FD*, having the sense coming from the algebraic difference itself.

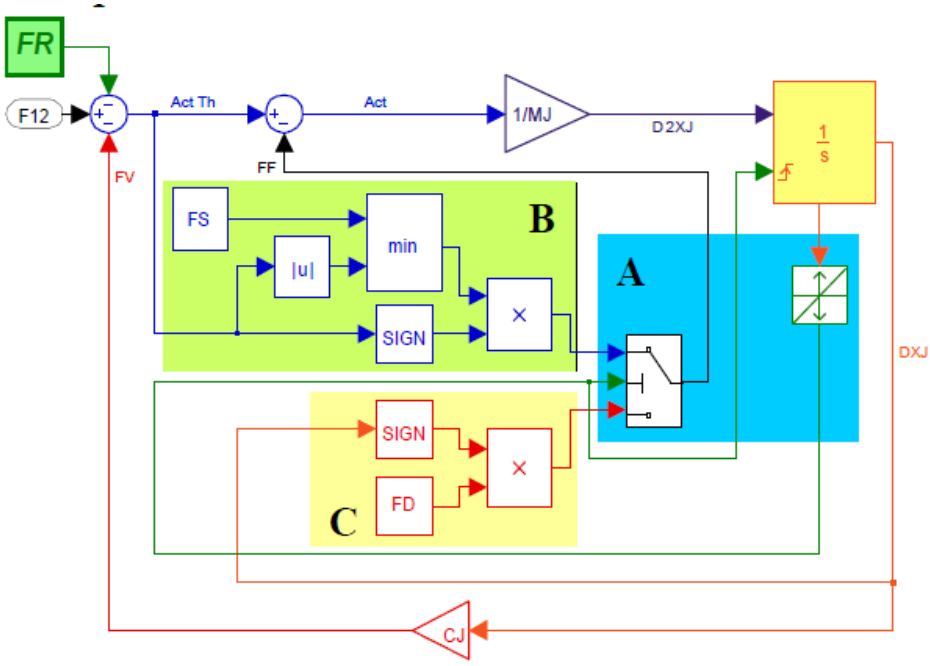

Figure 4.3 Representation of the Matlab- Simulink Friction force/torque algorithm presented by [11]

4.2.4 The influence of friction

This section shows the frictional effect on the mathematical model proposed, in figure 4.4 is shown the torque applied by the motor system and the response in terms of body pitch angle for an initial disturbance of 3º.

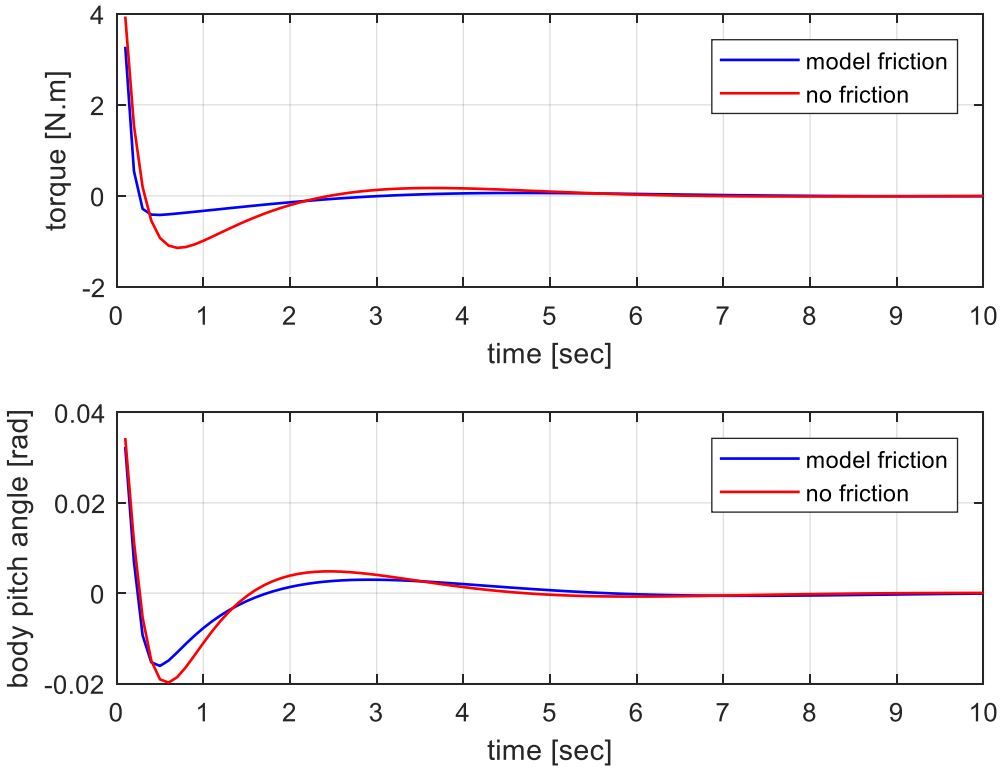

Figure 4.4 Comparation between friction and frictionless models for an initial disturbance of body pitch angle.

It shows how the system stabilization is positively influence by taking into consideration the friction in the model, this means that in the presence of an equal disturbance the friction model will have a less aggressive response, also is verified that the motor system will have a less expensive actuation with friction consideration. In figure 4.5 is shown the response on terms of delivered torque for a velocity tracking

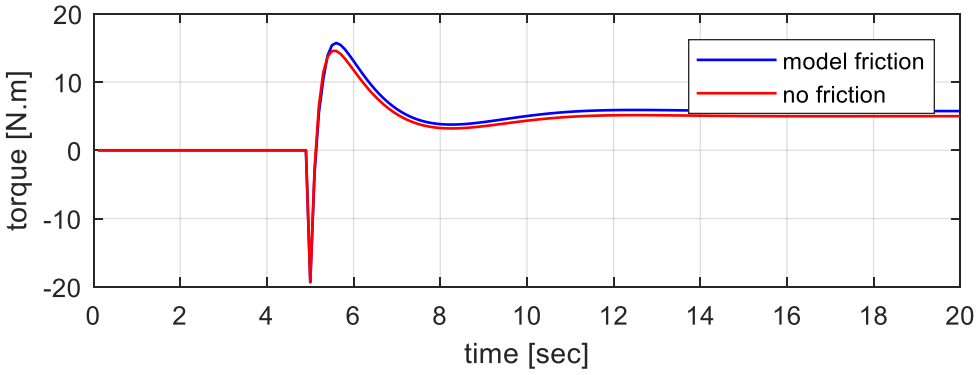

Figure 4.5 Torque delivered by the motor system for an initial disturbance of body pitch angle.

It is exposed how, at the end of the transitional period, will remain a difference of near 2 Nm between the torque that the system must really deliver to the torque of the frictionless system, this difference is the friction torque that the real system must overcome in order to keep a constant velocity.

4.2.5 Non-linearity analysis

It is important to analyze the role played by introducing a non-linear phenomena such as friction in the mathematical model, it is clear from the equation 4.5 that the value of the rolling friction coefficient and therefore the friction force, is directly proportional to the square of the angular velocity. The figure 4.6 shows the effect of angular velocity in the non-linearity behavior.

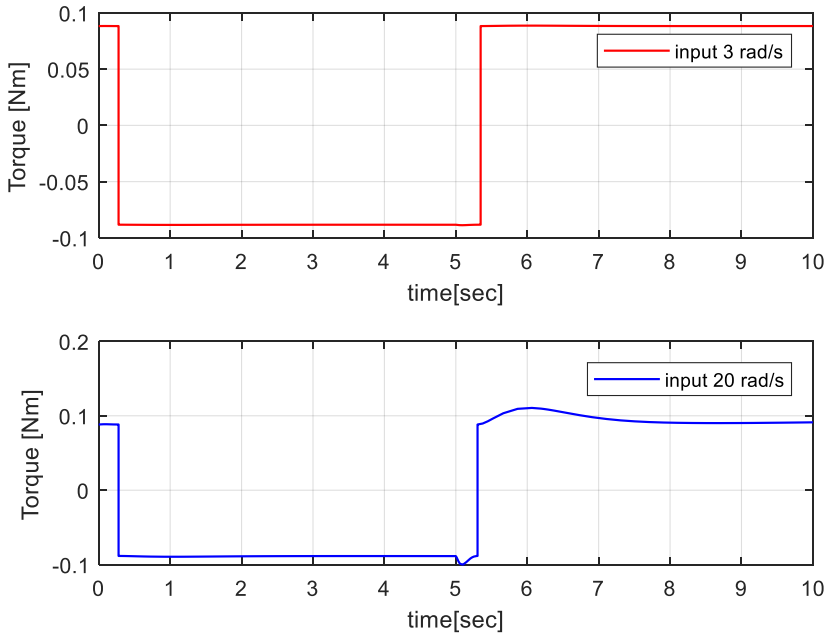

Figure 4.6 Friction Torque for a step velocity input

It follows how the influence of non-linearity is notable for values greater than 20 rad / sec. In the cases analyzed in chapter 1, it can be highlighted that a prototype of Ballbot rarely exceeds 7 rad/sec, therefore for future developments, could be adopted a linear model of friction.

4.3 Non-Zero floor slope

So far it has been considered that the Ballbot moves on a completely smooth surface, however, this situation is not usually presented in a real human environment, the performance analysis with a floor slope is crucial to expand the possible applications of the Ballbot.

This problem has been treated by Prof. Ralph Hollis in [13]. Working with an analogous approach, it will be possible to arrive to the equations that describe the dynamic behavior of the Ballbot.

4.3.1 Modeling

As first assumption is considered the slope angle as constant, at least in parts, and the slope is defined as the angle between the horizontal and the ground, where a positive slope means that the elevation of the floor decreases in the positive X direction.

The equations of motion have been developed using the Lagrangian method as the work done in 4.1. Considering for this case a new coordinate system X'Z' whereas, X 'is coincident with the ground.

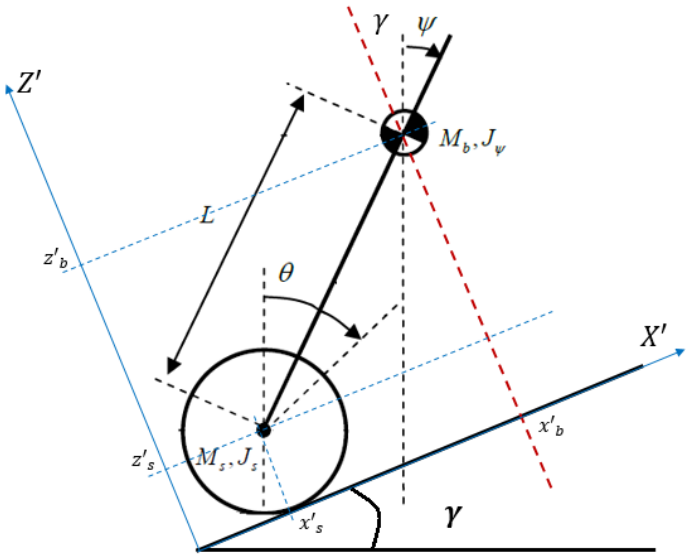

Figure 4.7 Bi-dimensional coordinate system for non-zero flor slope

Expressing the energies involved in this problem, The translational kinetic energy

$$T_1 = \frac{1}{2}M_s\left(R_s\dot{\theta}\right)^2 + \frac{1}{2}M_b\left(\left(R_s\dot{\theta} + L\,\dot{\psi}\cos(\gamma-\psi)\right)^2 + \left(L\,\dot{\psi}\sin(\gamma-\psi)\right)^2\right)$$

The Rotational kinetic energy

$$T_2 = \frac{1}{2}J_s\dot{\theta}^2 + \frac{1}{2}J_\psi\dot{\psi}^2$$

And the potential energy

$$U = M_s g z'_s + M_b g L\cos(\gamma-\psi)$$

Taking theta (θ) and psi (ψ) as system degrees of freedom, it is possible to obtain the equations of motions using the Lagrange's equations of the second kind.

$$\frac{d}{dt}\left(\frac{\partial L}{\partial \dot{\theta}}\right) - \frac{\partial L}{\partial \theta} = F_\theta$$

$$\frac{d}{dt}\left(\frac{\partial L}{\partial \dot{\psi}}\right) - \frac{\partial L}{\partial \psi} = F_\psi$$

Using a calculation routine built in Wolfram Mathematica, it is possible to arrive to the expression:

$$\mathrm{E}\begin{bmatrix}\ddot{\theta}\\ \ddot{\psi}\end{bmatrix} + F\begin{bmatrix}\dot{\theta}\\ \dot{\psi}\end{bmatrix} + G\begin{bmatrix}\theta\\ \psi\end{bmatrix} = \begin{bmatrix}C_M\\ 0\end{bmatrix}$$

Where

$$\mathrm{E}= \begin{bmatrix} a & b.\cos(\gamma-\psi) \\ a + b.\cos(\gamma-\psi) & c + b.\cos(\gamma-\psi)\end{bmatrix}$$

$$\mathrm{F}= \begin{bmatrix} 0 & -b.sin(\gamma-\psi)\dot{\psi} \\ 0 & -b.\sin(\gamma-\psi)\dot{\psi}\end{bmatrix}$$

$$\mathrm{G}= \begin{bmatrix} -d.sin(\gamma) \\ -d.\sin(\gamma) - gl_c m_b \sin(\psi)\end{bmatrix}$$

With

$a = r^2(m_b + m_B) + I_B$

$\mathrm{b} = rl_c\, m_B$

$c = I_B + l_c^2 m_B$

$d = g\, r(m_b + m_B)$

Isolating the variables $\ddot{\theta}$ e $\ddot{\psi}$ as follows:

$$\begin{bmatrix}\ddot{\theta}\\ \ddot{\psi}\end{bmatrix} = M^{-1}\left[\begin{bmatrix}C_M\\ 0\end{bmatrix} - C\begin{bmatrix}\dot{\theta}\\ \dot{\psi}\end{bmatrix} - G\begin{bmatrix}\theta\\ \psi\end{bmatrix}\right]$$

It is possible to arrive at

$$\ddot{\theta}=\frac{1}{ac-b^2\cos(\gamma-\psi)}\left(c\,C_M + b\,C_M\cos(\gamma-\psi) + b\,c\sin(\gamma-\psi)\dot{\psi}^2 + c\,d\sin(\gamma) - b\,g\,l_c\,m_b\sin(\psi)\cos(\gamma-\psi)\right)$$

$$\ddot{\psi}=\frac{1}{ac-b^2\cos(\gamma-\psi)}\left(a\,g l_c m_b\sin(\psi) - b\,d\sin(\gamma)\cos(\gamma-\psi) - a\,C_M + b^2\sin(\gamma-\psi)\cos(\gamma-\psi)\,\dot{\psi}^2\right)$$

4.4 Three-dimensional Model

So far, the coupling effects between the planar systems were neglected. This implies that if the Ballbot is moving in one direction, a sudden change of route does not involve any effects in the new course, this behavior does not represent the performance of the real system and therefore it is necessary consider a better physical model.

In this section It will be appropriately analyzed the Three-dimensional System considering the complete geometry and taking into account physical parameters simplified in previous sections. The purpose of this section is assessing the effects of the choice of a model and What role will the simplifications play in the final model.

4.4.1 Geometric Description

The Three-dimensional representation of the Ballbot (figure 4.7) could be construed as the union of five solids:

- The main body
- Three motor plants: consistent in electric motor and omnidirectional wheel
- The sphere

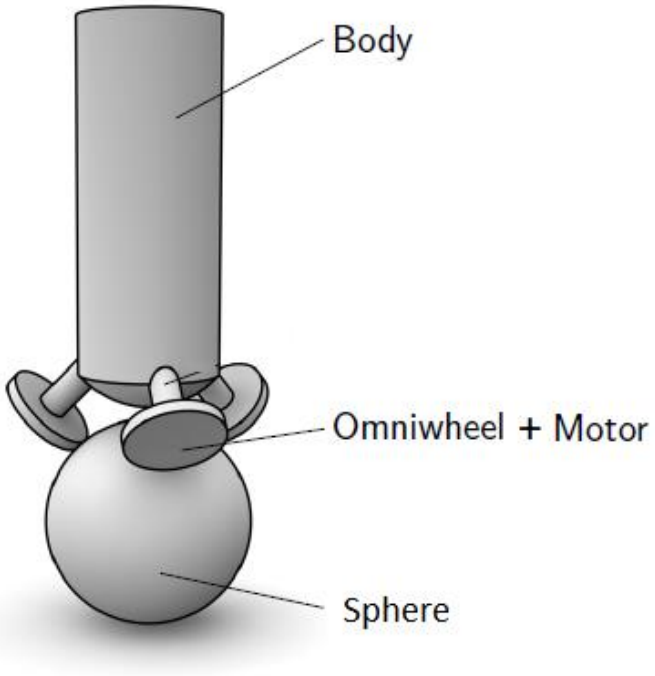

Figure 4.8 Three-dimensional Model adopted by [6]

We also consider the following simplifying hypothesis.

- There is no slip between the sphere and the ground.
- The rotation might be only in planes perpendicular to the ground, namely, there is no rotation in the vertical axis.
- Omnidirectional wheels are always in contact with the sphere.

4.4.2 Kinetic relationship

In order to express the kinetic relationship of the Ballbot its necessary to define a Coordinate system to write the orientation of the body in Euler Angles, in this case is consider the same representation adopted by Peter Fankhauser in [14], figure 4.8.

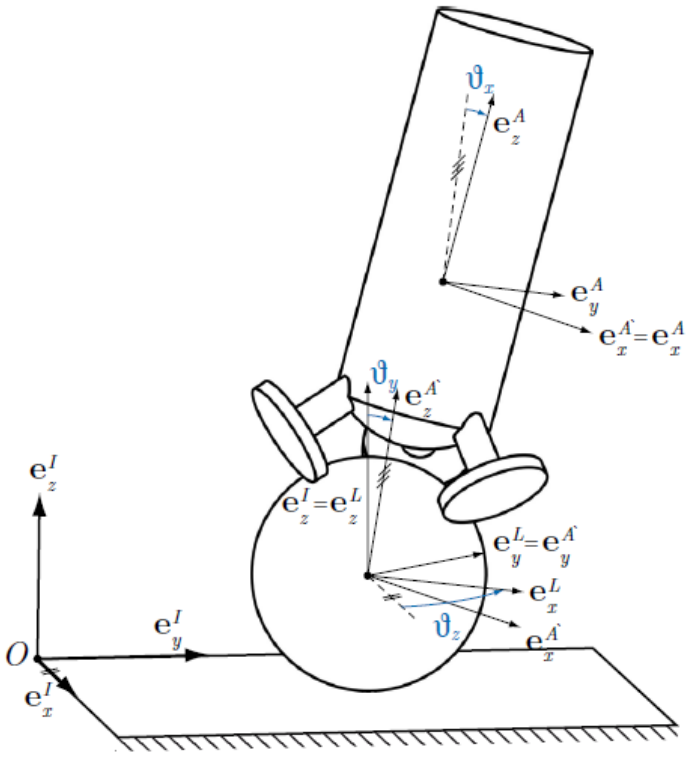

Figure 4.9 Coordinate system [14]

The original Inertial frame is denoted as "I" and the three elemental rotations will occur about the rotating coordinate system, which changes its orientation after each elemental rotation, after the first rotation θ_y a new frame, called "L" arises, which is rotated again a θ_u to generate the frame "A'", the last rotation θ_y generate the final frame solidary to the body called "A".

The velocity vectors of the solids involved are denoted as follows:

- **Angular velocity of the sphere:**

  Relative to the frame L

$$\overline{\Omega_S} = \begin{bmatrix} \dot{\theta}_x \\ \dot{\theta}_y \\ 0 \end{bmatrix}$$

- **Angular velocity of the omniwheels**

  In direction of the wheel axis and referenced to the system A

$$\omega_{OWi} = \dot{\psi}_i \qquad i = 1,2,3$$

  Furthermore, to express the absolute angular speed of the omniwheels in the body reference frame about the motor axis it is necessary to write

$$\overline{\Omega_{OWi}} = \omega_{OWi} + \frac{\overline{MW_i}}{\left|\left|\overline{MW_i}\right|\right|}\overline{\Omega_B}$$

  Where $\overline{MW_i}$ represent the distance between the node of the motor axis to the center point of the wheel I, and $\overline{\Omega_B}$ is the angular velocity of the body in the frame A.

- **Angular velocity of the body**

  To indicate the angular velocity of the body with the angles $\theta_z, \theta_y, \theta_x$ it is necessary to use the Jacobian matrix and the Euler angles $\dot{\bar{\theta}}$.

$$\overline{\Omega_B} = \bar{J}.\bar{\theta} = \begin{bmatrix} \dot{\theta}_x - \sin(\theta_y) \cdot \dot{\theta}_x \\ \cos(\theta_x) \cdot \dot{\theta}_y + \cos(\theta_y) \cdot \sin(\theta_x) \cdot \dot{\theta}_z \\ -\sin(\theta_x) \cdot \dot{\theta}_y + \cos(\theta_x) \cdot \cos(\theta_x) \cdot \dot{\theta}_z \end{bmatrix}$$

- **Linear velocity of the sphere**

  If the contact point between the sphere and the ground is denoted as B and the center of the sphere is denoted as C the translational vector of the spher can be computed as.

$$\dot{\bar{r}}_p = \Omega_S \times \overline{BC}$$

4.4.3 Dynamics equations

Analogously to the planar system introduced in (4.2), the Lagrange equation are used to compute the equations of motion

$$\frac{d}{dt}\left(\frac{\partial L}{\partial \dot{q}}\right) - \frac{\partial L}{\partial q} = F_{NP}$$

Where L represents the energies of the system

$$L = T_B + T_S + T_{W1} + T_{W2} + T_{W3} - U$$

- T_B: Kinetic energy of the body

$$T_B = \frac{1}{2}\, m_B\, \dot{\bar{r}}_p^{\,T}\, \dot{\bar{r}}_p + m_B\, \left(\bar{R}_{AI} \cdot \dot{\bar{r}}_p\right) \cdot \left(\overline{\Omega_B} \cdot \dot{\bar{r}}_p\right) + \frac{1}{2}\, \overline{\Omega_B}^{T}\, \overline{I_B}\, \overline{\Omega}_B$$

- T_s: Kinetic energy of the sphere

$$T_K = \frac{1}{2}\, m_S\, \dot{\bar{r}}_p^{\,T}\, \dot{\bar{r}}_p + \frac{1}{2}\, \overline{\Omega_S}^{T}\, \overline{I_S}\, \overline{\Omega}_S$$

- T_{Wi}: Kinetic energy of the omniwheel i (i=1,2,3)

  We consider only the rotational energy of the omniwheel and the motor

$$T_{OW} = \frac{1}{2}\, \overline{I_{OW}} \quad \overline{\Omega_{OW\iota}}^{2}$$

- U: Potential energy

$$V_B = -m_B\, \bar{G}\, \bar{R}_{AI} \dot{\bar{r}}_p$$

The term "q" caracterized the minimal coordinates represented by

$$\bar{q} = \left[\theta_x, \theta_y, \psi_x, \psi_y, \psi_Z\right]$$

And F_{NP} represents the non potencial forces, in this case the motor torques acting directly in each omniwheel called T

4.4.2 Linearization of the model

The Lagrange equations that represent the dynamics of the System are solved by computing system, due to the size of this equations, its study is limited to a linearized equation, using a state space representation as in section 4.1.4 it is possible to write

$$\dot{x} = A\bar{x} + B\bar{u}$$

$$y = C\bar{x} + D\bar{u}$$

Where the state vector is:

$$\bar{x} = \left[\theta_x \dot{\theta}_x, \theta_y, \dot{\theta}_y, \psi_x, \dot{\psi}_x, \psi_y, \dot{\psi}_y, \psi_Z, \dot{\psi}_Z\right]^T$$

And the input vector is characterized by the motor torque applied to each omniwheel

$$u = \begin{bmatrix} T_1 \\ T_2 \\ T_3 \end{bmatrix}$$

As a first approach was taken the unstable equilibrium position ($\psi = 0$) as a point of linearization, this outcome in the following state matrix

$$A_0 = \begin{bmatrix} 0 & 1 & 0 & 0 & 0 & 0 & 0 & 0 & 0 & 0 \\ 52 & 0 & 0 & 0 & 0 & 0 & 0 & 0 & 0 & 0 \\ 0 & 0 & 0 & 1 & 0 & 0 & 0 & 0 & 0 & 0 \\ 0 & 0 & 52 & 0 & 0 & 0 & 0 & 0 & 0 & 0 \\ 0 & 0 & 0 & 0 & 0 & 1 & 0 & 0 & 0 & 0 \\ 0 & 0 & 0 & 0 & 0 & 0 & 0 & 0 & 0 & 0 \\ 0 & 0 & 0 & 0 & 0 & 0 & 0 & 1 & 0 & 0 \\ -52 & 0 & 0 & 0 & 0 & 0 & 0 & 0 & 0 & 0 \\ 0 & 0 & 0 & 0 & 0 & 0 & 0 & 0 & 0 & 1 \\ 0 & 0 & -52 & 0 & 0 & 0 & 0 & 0 & 0 & 0 \end{bmatrix}$$

Analyzing the matrix A_0 , it is possible notice that the system presents three subsystems linearly independent, corresponding to the three spatial planes, they are presented in one decupled system corresponding to the yz plane and two identical pairs corresponding to yz and xz planes, equality is due to the perfect symmetry adopted in this phase of design.

For the control matrix was computed the following result

$$B_0 = \begin{bmatrix} 0 & 0 & 0 \\ 6.2 & -3.1 & -3.1 \\ 0 & 0 & 0 \\ 0 & 0 & 0 \\ 0 & 3.1 & -3.1 \\ 0 & 0 & 0 \\ 0 & 0 & 0 \\ -15.2 & 8.48 & 8.48 \\ 0 & 0 & 0 \\ 0 & -12.5 & -12.5 \end{bmatrix}$$

Next, it is interesting to study a linearization for an arbitrary point such as

$$\bar{x} = [\dot{\theta}_x, \dot{\theta}_y, \psi_x, \dot{\psi}_x, \psi_y, \dot{\psi}_y, \dot{\psi}_Z]^T = \left[4\frac{rad}{s}, 8\frac{rad}{s}, 0.3rad, -0.5\frac{rad}{s}, 0.2rad, 0.4\frac{rad}{s}, 0.4\frac{rad}{s}\right]^T$$

For this case we will obtain the following matrices

State matrix:

$$A_i = \begin{bmatrix} 0 & 1 & 0 & 0 & 0 & 0 & 0 & 0 & 0 & 0 \\ 15.3 & -0.8 & 72 & 1.2 & 0 & 4.2 & 0 & 0.03 & 0 & 0.12 \\ 0 & 0 & 0 & 1 & 0 & 0 & 0 & 0 & 0 & 0 \\ -70.5 & 4.12 & 25.3 & -8.4 & 0 & -5.4 & 0 & -0.8 & 0 & -1.2 \\ 0 & 0 & 0 & 0 & 0 & 1 & 0 & 0 & 0 & 0 \\ -40.2 & -10.2 & 4.2 & 25 & 0 & 6.8 & 0 & 1.86 & 0 & 2.2 \\ 0 & 0 & 0 & 0 & 0 & 0 & 0 & 1 & 0 & 0 \\ -15.2 & -3 & -32.15 & 1.64 & 0 & -2.68 & 0 & 0.03 & 0 & 0.30 \\ 0 & 0 & 0 & 0 & 0 & 0 & 0 & 0 & 0 & 0 \\ 52.2 & 0.45 & -43.6 & -5.01 & 0 & 5.1 & 0 & -0.58 & 0 & -0.4 \end{bmatrix}$$

Control Matrix:

$$B_i = \begin{bmatrix} 0 & 0 & 0 \\ 3.8 & -4.2 & -4.2 \\ 0 & 0 & 0 \\ 4.58 & 8.12 & 3.2 \\ 0 & 0 & 0 \\ -15.25 & -8.95 & -16.51 \\ 0 & 0 & 0 \\ -15.39 & 10.52 & 10.52 \\ 0 & 0 & 0 \\ -6.1 & -15.2 & 9.6 \end{bmatrix}$$

These results show that a model based on a linearization point other than the equilibrium point, presents strong terms of coupling between planes and from this it follows that the two-dimensional model, proposed in section 4.1 will respond with accurate outcomes at operating points where all states are nearby zero.

From this point forward, the two-dimensional model will be adopted under the assumption of small angles.

Chapter 5 - Controller Design

5.1 Control properties

Once the space state system has been defined with the dynamic modeling of the previous chapter, we propose to design a control system capable of stabilizing the Ballbot. To achieve this goal, it is necessary first, analyze two important system properties, controllability and observability.

5.1.1 Controllability

Controllability of a system is its ability to reach any state value manipulating only the input vector i.e. that an arbitrary configuration of the body pitch angle(ψ) and the sphere rotation angle (θ) is reachable by acting with a proper input torque. Consider for this case the continuous linear system:

$$\dot{x} = A\bar{x} + Bu$$
$$y = C\bar{x}$$

Where:

- $\bar{x}$ is the $[4 \times 1]$ state vector, y is the $[4 \times 1]$ output vector and u is the $[1 \times 1]$ control vector.
- A is the $[4 \times 4]$ state matrix, B is the $[4 \times 1]$ control matrix and C is the $[4 \times 4]$ output matrix.

Thus, it is possible to define the $[4 \times 4]$ controllability matrix R as follows

$$R = [B \quad AB \quad A^2B \ \ldots \ A^{n-1}B]$$

The system will be controllable if the R matrix has full row rank i.e. $Rank(R) = 4$. For the system proposed in the previous section the controllability matrix is given by

$$R = \begin{bmatrix} 0 & 10{,}15 & -156{,}99 & 2571{,}55 \\ 0 & 2571{,}55 & 82{,}06 & -1401{,}02 \\ 10{,}15 & -156{,}99 & 2571{,}55 & -42566{,}4 \\ -5{,}30 & 82{,}06 & -1401{,}0 & 23128{,}87 \end{bmatrix}$$

Using the MATLAB command *ctrb* we can obtain the controllability matrix and verify that the system is controllable.

5.1.2 Observability

Observability give us an idea of how states of the system can be measured from of its external outputs. Formally, a system is observable if, for any arbitrary state and control vectors, the current state can be computed in finite time using the output.

Considering the system defined in (5.1.1)

$$\dot{x} = A\bar{x} + Bu$$

$$y = C\bar{x}$$

The observability matrix is defined as follows

$$C = [C \quad CA \quad CA^2 \ \ldots \ CA^{n-1}]$$

If the row rank of the following observability matrix $Rank(C)$ is equal to the number of state variables, then the system is observable. Using the MATLAB command *obsv* we can obtain the observability matrix and verify that the system observable i.e. $Rank(R) = 4$

4.1.3 Open-Loop Analysis

Before connecting the feedback signals, let's Perform some open-loop analysis to project possible control approaches. It is known that the system is naturally unstable, this means that in the face of a disturbance the body will inevitably fall.

It is possible to base this behavior analyzing the poles of a system. We will specifically study the poles of the system using the MATLAB function `pzmap`. The poles of the system where the pitch angle is the output are found as shown below:

$$p = \begin{bmatrix} 0 \\ -16.5687 \\ 3.1737 \\ -2.0665 \end{bmatrix}$$

The pole at 3.173 the pole has positive real part, this is due to system instability. Analyzing the pole-zero map in Figure 4.1 we note how the pole is in the right half of the complex s-plane. This confirm what we observed above.

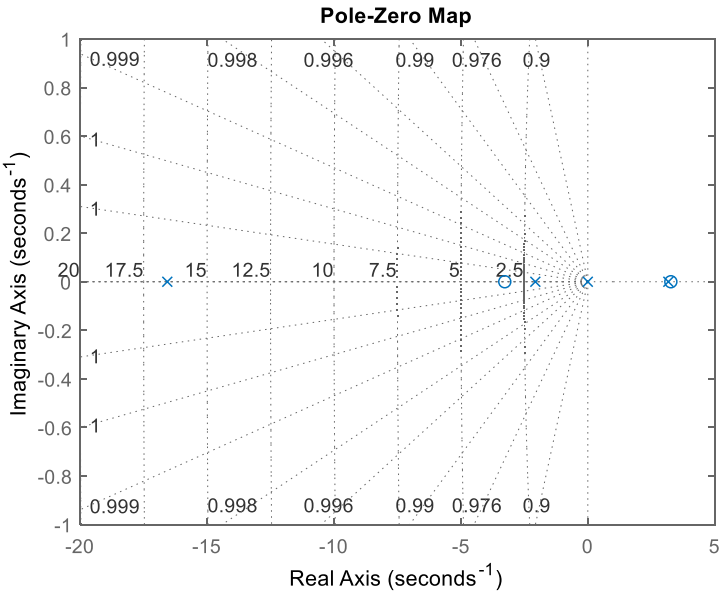

Figure 5.1: Pole Zero Map for the open loop system

5.2 LQR control

Huibert Kwakernaak (1972) claims [15] that a time-invariant linear system under a condition of complete controllability system can always be stabilized by a linear feedback law. In fact, more can be done. Because the closed-loop poles can be located anywhere in the complex plane, the system can be stabilized; but, moreover, by choosing the closed-loop poles far to the left in the complex plane, the convergence to the zero state can be made arbitrarily fast. To make the system move fast, however, large input amplitudes are required. In any practical problem the input amplitudes must be bounded; this imposes a limit on the distance over which the closed-loop poles can be moved to the left. These considerations lead quite naturally to the formulation of an optimization problem, where we consider both the speed of convergence of the state to zero and the magnitude of the input amplitudes.

Therefore, in order to design a control with a good compromise between the speed of convergence and the energy expended by the system a control is implemented with the LQR (Linear Quadratic Regulator) technique, this method is based on the manipulation of matrix equations, using the control and state matrices and weighting factors chosen by the designer according to his criteria evaluating the performance of the control system.

5.2.1 LQR Methodology

Given the continuous-time linear system in a state space representation as follows

$$\begin{cases} \dot{x} = A\bar{x} + Bu \\ \quad y = C\bar{x} \end{cases}$$

The LQR technique is based on determining the feedback gain matrix K (where $u = -Ky$) that minimizes the value of a quadratic performance index (PI). The minimization of this PI or cost function must guarantee system stability and good time response, the PI is defined as:

$$J = \frac{1}{2}\int_0^\infty (\bar{x}Q\bar{x}^T + \bar{u}R\bar{u}^T)$$

where Q and R are the weighting factors. Q and R non-negative definite symmetric matrices, this implies a positive value of J and consequently design of the control system is transformed into a minimization problem of the cost function; in other words, we want to minimize the energy fed into the system by commands over time.

In the case where $R \gg Q$ the cost function is weighted by the control effort u, then the regulator focuses on minimizing the control action this could be consider as an expensive control solution. Conversely if $Q \gg R$ the cost function is weighted by the state errors and the system's response becomes arbitrarily fast.

Once the weight matrices have been defined, the K matrix will be compute by means of numerical techniques with the assistance of the MATLAB function `lqr()`.

5.3 Velocity tracking

Consider the state system introduced which describes the dynamic behaviour of the system

$$\begin{cases} \dot{x} = A\bar{x} + Bu \\ \quad y = C\bar{x} \end{cases}$$

Whereas the state vector is defined as:

$$\bar{x} = [\theta, \psi, \dot{\theta}, \dot{\psi}]$$

Now a state variable is defined as control variable to ensure the controllability of the System. In this case, by assuming θ as reference variable. Besides, an error function is defined as the difference between the measured signal and the reference one.

$$e_{(t)} = \theta_{(t)} - \theta_{rif}$$

Now, a new variable z is added. This variable is defined as the integral of the error, as follows:

$$z_{(t)} = \int e_{(t)} \quad = \int (\theta_{(t)} - \theta_{rif}) \tag{5.1}$$

The next step is the definition of an augmented system (AG) formed by the state vector $\bar{x}$ and the variable $z_{(t)}$.

$$\begin{bmatrix} \dot{x}_{(t)} \\ \dot{z}_{(t)} \end{bmatrix} = \begin{bmatrix} A & 0 \\ C_\theta & 0 \end{bmatrix} \begin{bmatrix} x_{(t)} \\ z_{(t)} \end{bmatrix} + \begin{bmatrix} B \\ 0 \end{bmatrix} u_{(t)} - \begin{bmatrix} 0 \\ I \end{bmatrix} C x_{rif} \tag{5.2}$$

The equation (4.2) converges to the equation (4.3) if the Augmented System is assumed as stable.

$$\begin{bmatrix} \dot{x}_{(\infty)} \\ \dot{z}_{(\infty)} \end{bmatrix} = \begin{bmatrix} A & 0 \\ C_\theta & 0 \end{bmatrix} \begin{bmatrix} x_{(t)} \\ z_{(t)} \end{bmatrix} + \begin{bmatrix} B \\ 0 \end{bmatrix} u_{(t)} - \begin{bmatrix} 0 \\ I \end{bmatrix} C x_{rif} \tag{5.3}$$

The state equation of the Augmented System could be obtained by the subtraction between (4.2) and (4.3).

$$\begin{bmatrix} \dot{x}_{AG(t)} \\ \dot{z}_{AG(t)} \end{bmatrix} = \begin{bmatrix} A & 0 \\ C_\theta & 0 \end{bmatrix} \begin{bmatrix} x_{AG(t)} \\ z_{AG(t)} \end{bmatrix} + \begin{bmatrix} B \\ 0 \end{bmatrix} u_{AG(t)} \tag{5.4}$$

Or in the state space representation:

$$\dot{\bar{x}}_{AG} = \bar{A}_{AG}\bar{x}_{AG} + \bar{B}_{AG}\bar{u}_{AG}$$

Reminding that the x_{AG} z_{AG} variables were defined as:

$$x_{AG} = x_{(t)} - x_{(\infty)}$$
$$z_{AG} = z_{(t)} - z_{(\infty)}$$

At this point it is possible to apply the LQR technique, defined in the previous section 5.2.1, taking into account that is required to consider the parameters $\bar{A}_{AG}$ and $\bar{B}_{AG}$ as state and control matrix of the system, respectively.

Once computed a gain matrix K, it is possible to write the input of the system as shown in the following equation.

$$\bar{u}_{AG} = K\bar{x}_{AG} = K_f x_{AG} + K_i z_{AG} = K_f\left(x_{(t)} - x_{(\infty)}\right) + K_i(z_{(t)} - z_{(\infty)})$$

It is important to remember the definition of $z_{(t)}$ that was described in (5.1). By tending both, $x_{(\infty)} \to x_{rif}$ and $z_{(\infty)} \to 0$, the input of the system will be:

$$\bar{u}_{(t)} = K_f\left(x_{(t)} - x_{rif}\right) - K_i \int \left(\theta_{(t)} - \theta_{rif}\right) dt$$

5.4 Controller gains calculation

In LQR theory there is no a standard technique to choose the values of Q and R in the cost function (equation 5.1), instead, an empirical technique is used based on the experimentation and observation of the results.

$$J = \frac{1}{2}\int_0^\infty (\bar{x}Q\bar{x}^T + \bar{u}R\bar{u}^T) \qquad (5.1)$$

A first approach may be computed using the Bryson's Rule [16] to achieve a selective penalization of the states. In this technique Q and R are chosen as diagonal matrix with

$$Q_{ii} = \frac{1}{e_{i,max}^2}$$
$$R_{ii} = \frac{1}{u_{i,max}^2}$$

Where $e_{i,max}^2$ is the square of the maximum acceptable error of the measured state i and $u_{i,max}^2$ is the square of the maximum aadmissible input. Reminding the section 3.1.2 where the control requirements were defined, the maximum acceptable error for the body pitch angle is chosen to be 10º, furthermore the maximum error for the sphere rotation angle, which represents the position of the Ballbot, is chosen to be 1 rad. For the derivatives of the states are taken the double of the errors of the respective states, which results in the following matrices.

$$Q = \begin{bmatrix} 1 & 0 & 0 & 0 & 0 \\ 0 & \frac{180^2}{(10\pi)^2} & 0 & 0 & 0 \\ 0 & 0 & 1 & 0 & 0 \\ 0 & 0 & 0 & \frac{180^2}{(20\pi)^2} & 0 \\ 0 & 0 & 0 & 0 & 1 \end{bmatrix}$$

As soon as input limits, it is proposed adopt a maximum of 30 Nm which corresponds to a nominal value of a stepper motor, then:

$$R = \frac{1}{30^2}$$

This lead to the following gain matrix:

$$K = [-5.75 \quad -208 \quad -6.02 \quad -46.23 \quad -3.16]$$

5.5 Simulink implementation

Firstly , the signal generator is built. Due to the control command will be the angular velocity of the sphere, it is necessary to integrate this signal in order to obtain the value of the reference variable θ_{rif}.

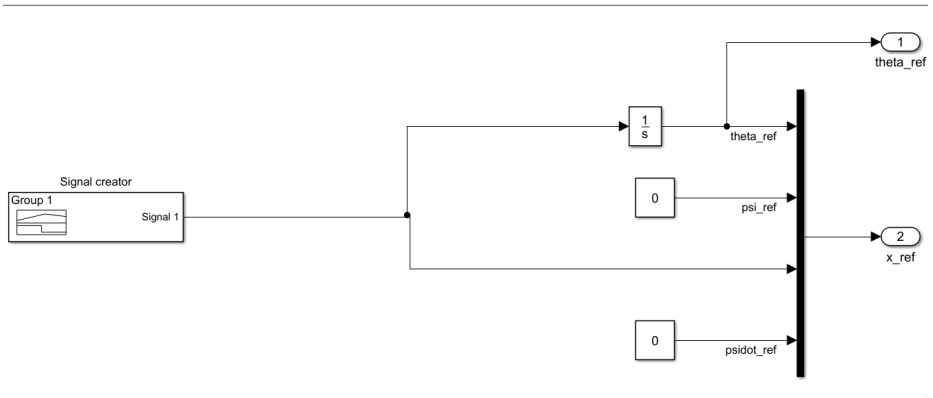

Figure 5.2: Signal generator block

In order to simplify the system, the reference generator was grouped into a subsystem, in which the outputs will be θ_{rif} and x_{rif}. Now, the development of the model requires to close both of the two control loops, the one that works in the state vector ensuring the stabilty and the other related to the signal θ_{rif} and makes the model to follow the velocity command.

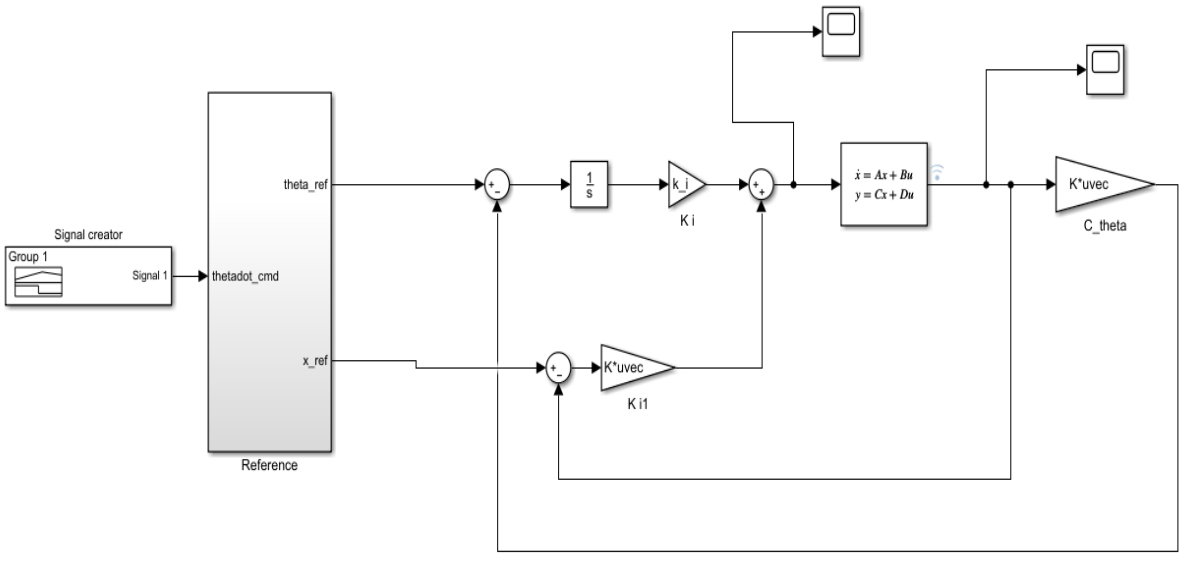

Figure 5.3: Complete system modeling

Finally, to demonstrate the functionality of the control system in Figure 5.4 it is prensented the response in terms of θ (rotation of the sphere, in, $\dot{\theta}$ (angular velocity of the spher) and body pitch angle φ to an initial distrubance.

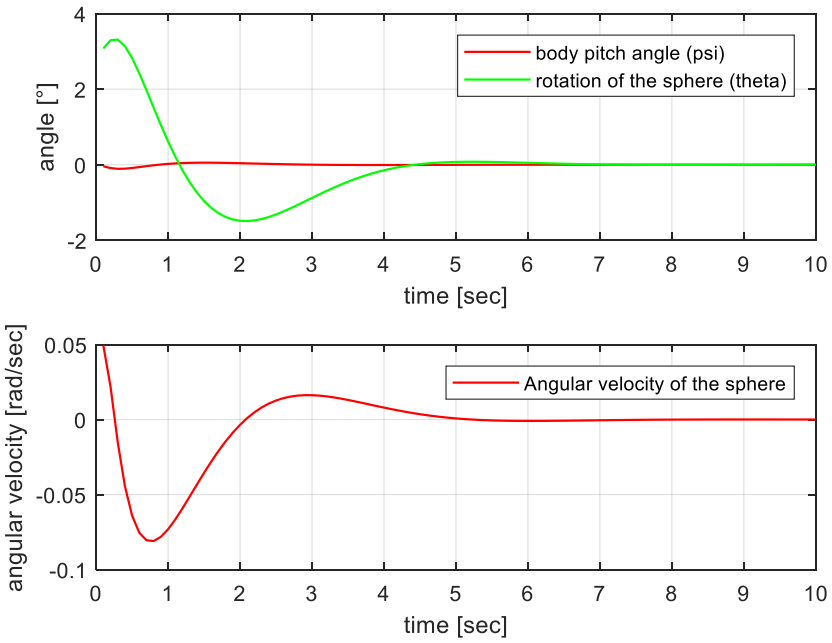

Figure 5.4 Initial disturbance response. rotation of the sphere, body pitch angle and angular velocity of the sphere,

Chapter 6 - The influence of design parameters

6.1 Mass influence

Let's see how the Ballbot responds to an increase in its weight, for this case is consider the model developed in chapter 4. In figure 6.1 in figure it is shown the response of the pitch body angle (psi) and ball angular velocity (theta_dot) to a step unitary input in velocity.

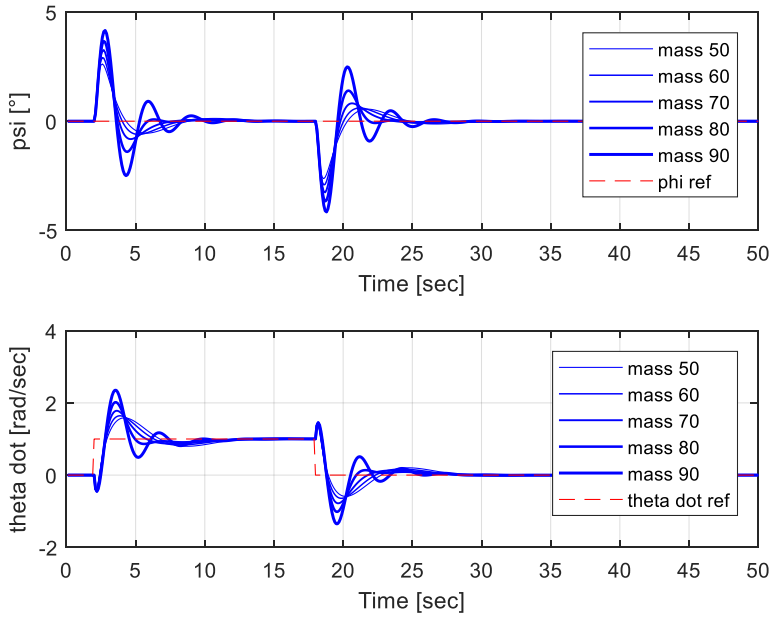

Figure 6.1 Mass variation for an step input on velocity tracking.

It is possible to see how an increase in mass negatively influences the stability of the system i.e. a longer settling time and a larger overshoot.

Likewise, it is important to note how the mass influences on the energy of the motor system in terms of torque (Figure 6.2), this implies that in order to move the Ballbot with a greater weight it will be necessary to use further energy, increasing the encumbrance of the system, battery and so on.

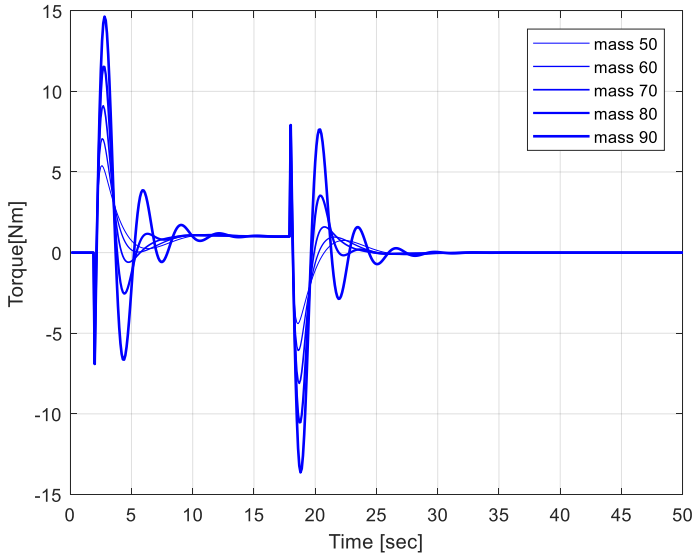

Figure 6.2 Torque of the motor system for mass variation

6.2.1 Mass Variation with a non-zero floor slope

Let's see an analogous analysis to the previous one with the consideration of different values in the floor slope.

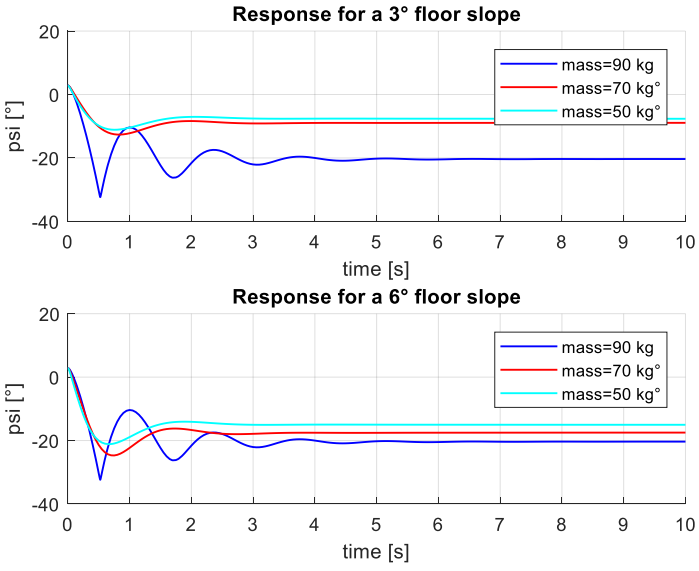

Figure 6.3 Body pitch angle response for mass variation with diferent floor slopes

Figure 6.3 shows how the increase in mass has a similar effect as in the case analyzed in section 6.1. Nonetheless, due to the presence of a floor slope, once the transitional is over, the body will keep a constant pitch angle in order to keep the system in balance, this angle will be a function of the slope angle and the mass.

6.2 COM distance influence

The COM (Center Of Mass) distance is one of the most important parameters in the design, because a small change in this parameter can result in large differences in a later state. Figure 6.4 shows the response of the system to a velocity tracking.

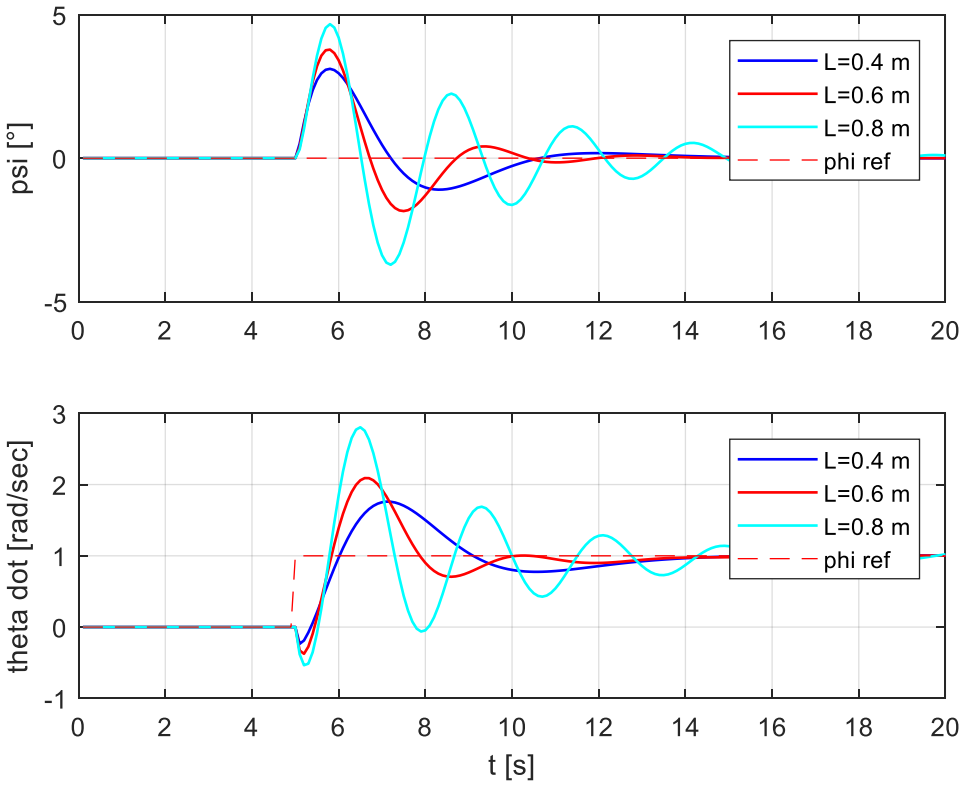

Figure 6.4 System Response for a COM distance variation

Analyzing the response of the body pitch angle (psi) it is possible to notice how an increase in the COM distance, influence negatively on the stability of the system, also

in the lower graph it shows how for an increase in the COM distance the velocity tracking presents a more pronounced oscillation with higher overshoots.

At other constant parameters we find a limit of L = 0.9m where from there the system becomes unstable

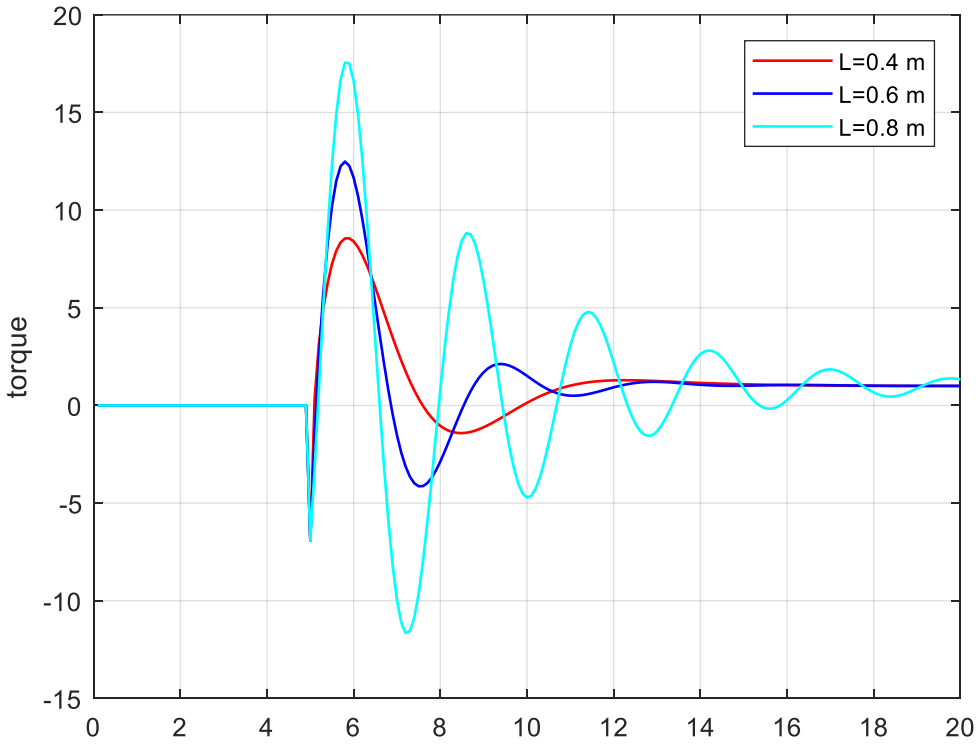

Figure 6.5 Torque of the motor system for a COM distance variation for a velocity tracking

Figure 6.5 shows an intuitive result considering the previous explanations, the outcome is that for a larger COM distance, the torque provided by the Motor System must be greater, the result is explained by the fact that the body has more energy kinetics to balance.

6.3 Floor slope isolated influence

In this section will be analyzed the behavior of the Ballbot for different floor slopes according to the model developed in the section 4.3. Figure 6.6 shows five different cases for the stabilization front of a disturbance of 3º degrees, the behavior is studied for slopes of $\pm 3º, \pm 6º$ and a 0º slope as reference case.

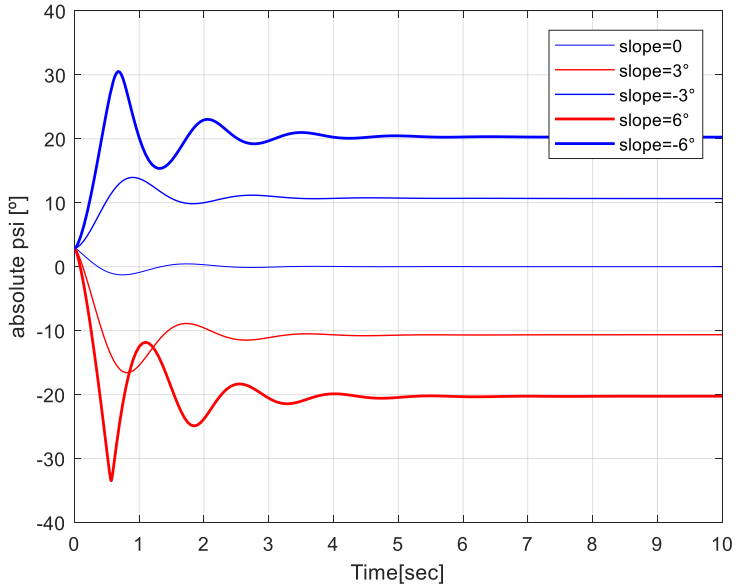

Figure 6.6 System response for a initial disturbance with floor slopes variations

It shows how an increase in the slope angle influences the stability of the system, that means, with an increase in pending it will be more difficult to stabilize the Ballbot it also stands out how the sign of pendency influences in the stabilization, reminding the convention adopted in section 4.3 a positive slope declines the terrain in the direction of the x-axis as indicated Figure 6.7, then, is highlighted the intuitive result that a positive slope helps stabilization for a negative disturbance.

$slope = \gamma > 0$ $slope = \gamma < 0$

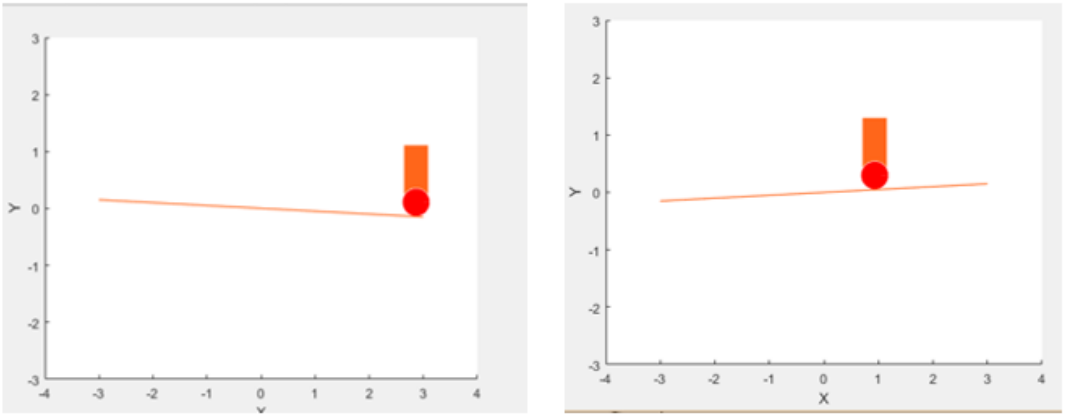

Figure 6.7 Slope sign convention

Chapter 7 - Case analysis and control optimization

In this chapter it will be considered two important motion profiles that could appear in the practical applications of the Ballbot

- Angular velocity step input of 1 3 y 5 rad/seg
- Trapezoidal input with maximum acceleration of 1 3 y 5 rad/seg^2

After analyzing each case, comparing them with the requirements proposed in chapter 3, a controller improvement was proposed in order to achieve a better performance taking care not to exceed the limits of power required.

7.1 Angular velocity step

In the first case it will be analyzed a velocity-step of 8 seconds of duration, this is equivalent to a linear displacement of the Ballbot, Figure 7.1 shows the response in terms of the angular velocity of the sphere, Figure 7.2 shows the body pitch angle and in Figure 7.3 displays the torque applied by the motor system.

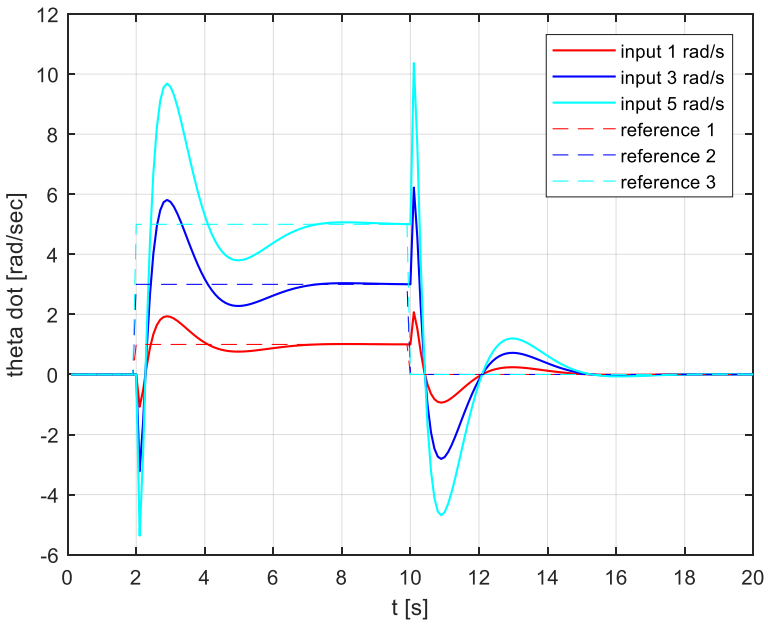

Figure 7.1 Angular velocity of the sphere for three different step inputs

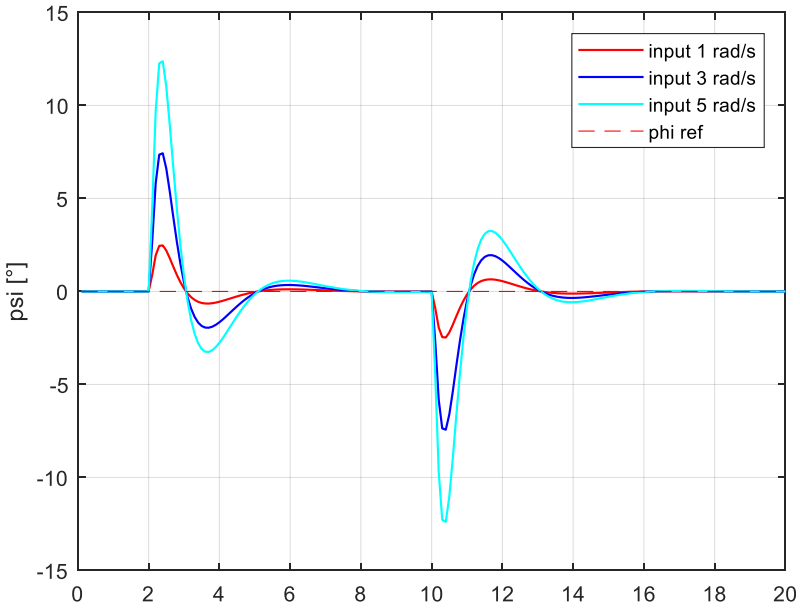

Figure 7.2 body pitch angle for three different step inputs

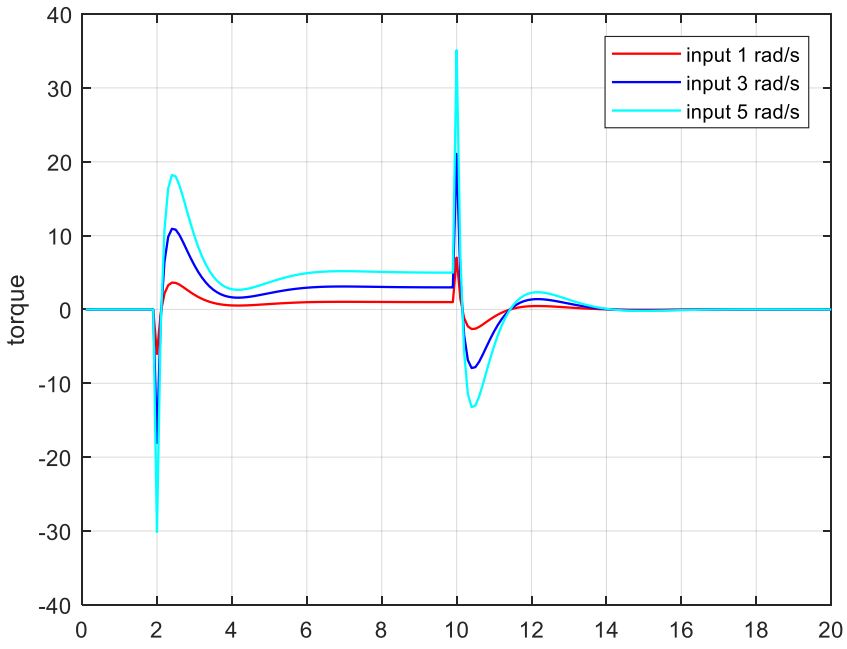

Figure 7.3 Torque provided by the motor system for three different step inputs

Analyzing the figure 7.1, it is noted that for the case of 5 rad/sec an excess in the body pitch angle is obtained, also for the same speed was find very high torque values in the deceleration of the Ballbot (Figure 7.3). These behaviors should be improved with an improvement in the control system. Table 7.1 summarizes the characteristic values of each response comparing them with the requirements introduced in the chapter 3.

Table 7.1 characteristic values and maximum requirements for a velocity step input

Case	Settling Time [s]		Overshoot on ψ [º]		Maximun Torque	
	value	Max.	value	Max.	value	Max.
1 rad/seg	4.2 sec	6 sec	2.1º	10º	$8Nm$	$30Nm$
3 rad/seg	4.8 sec		7.3º		21 Nm	
5 rad/seg	5 sec		12.8º		35 Nm	

7.2 Trapezoidal Input

This type of input is interesting to analyze to evaluate how the velocity tracking adapts to ramp input profile, in order to achieve this, three trapezoidal profiles with maximum accelerations of $1, 3\ and\ 5\ {}^{rad}/_{sec}$ were simulated. The responses in terms of angular velocity of the sphere, body pitch angle and the torque applied by the motor system are presented in Figure 7.4, 7.5 and 7.6 respectively.

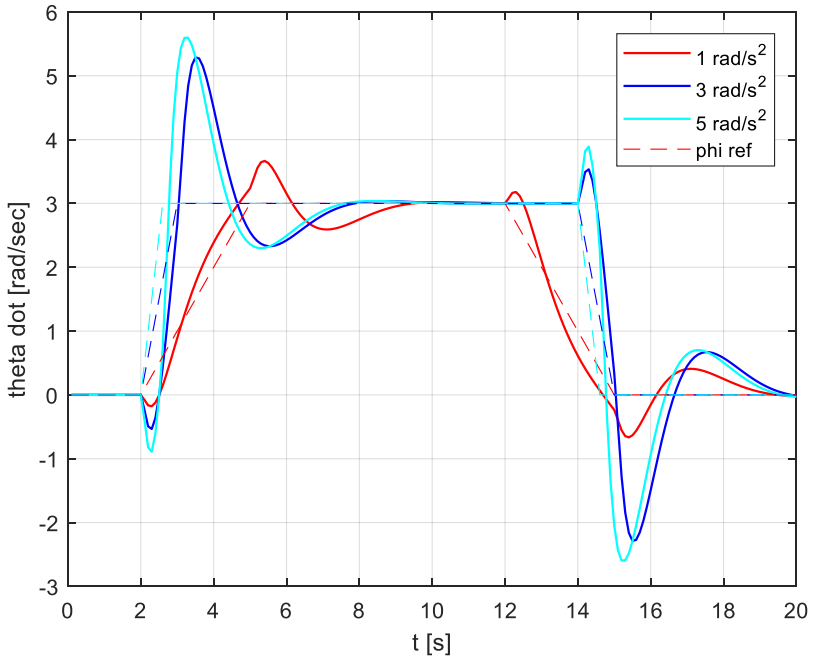

Figure 7.4 Angular velocity of the sphere for three acceleration profiles

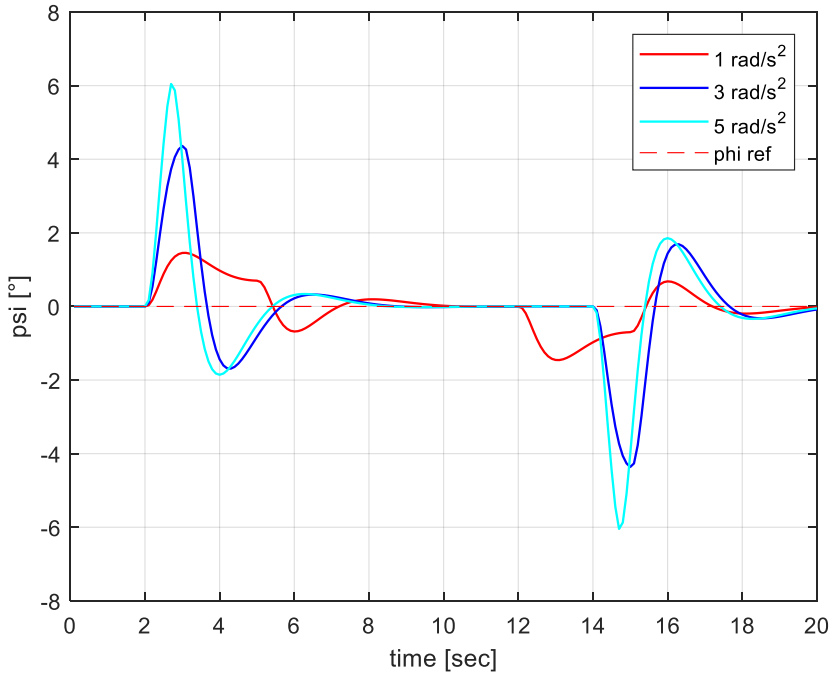

Figure 7.Body pitch angle for three acceleration profiles

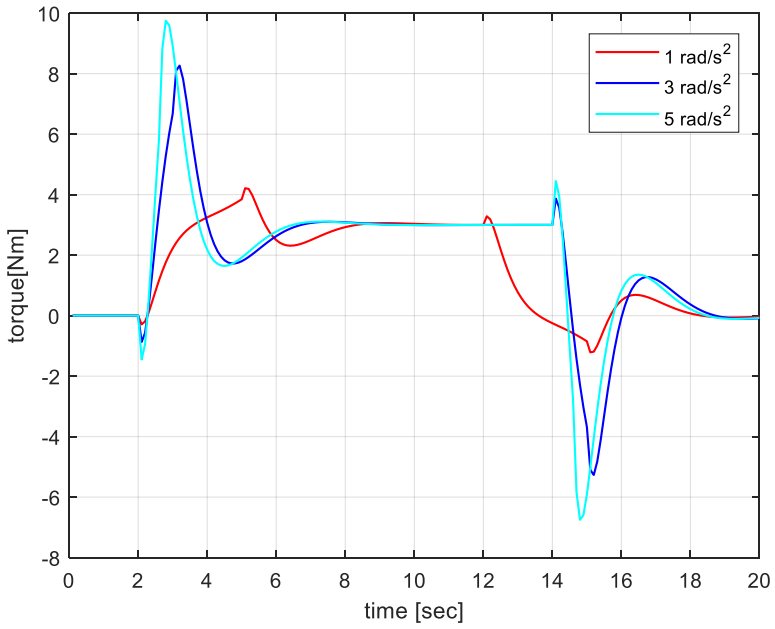

Figure 7.5 Torque provided by the motor system for three acceleration profiles

Analyzing figures 7.4, 7.5 and 7.6, and considering the limits proposed in chapter 3, it is noted that in the three cases the requirements are met, however, the tracking efficiency on the ramp it will improved, ensuring that the system follows the input path accordingly.

7.3 Controller improvement

The results presented so far were obtained with the controller proposed in section 5.4, this was a first approach for the gain matrix calculation, given the results of section 7.1 and 7.2 it is proposed modify the controller to improve the behavior of the system.

In order to do this, is required to adjust the weighting matrices of the function cost (equation 5.1). The adjustment will be made changing the factors relative to the body pitch angle and the tracking error, which results in the following matrix

$$Q = \begin{bmatrix} 1 & 0 & 0 & 0 & 0 \\ 0 & \frac{180^2}{(30\pi)^2} & 0 & 0 & 0 \\ 0 & 0 & 1 & 0 & 0 \\ 0 & 0 & 0 & \frac{180^2}{(60\pi)^2} & 0 \\ 0 & 0 & 0 & 0 & 6e3 \end{bmatrix}$$

Since most of the torque profiles are acceptable the value of R remains unchanged

This lead to the following gain matrix:

$$K = [-86.5 \quad -834 \quad -38 \quad 223 \quad -100]$$

7.5 Final results

Launching the simulations with the new control system defined in 7.4, the system shows a clear improvement, Figure 7.6 and 7.7 shows the comparison between the preliminary system and the improved system for slightest edge.

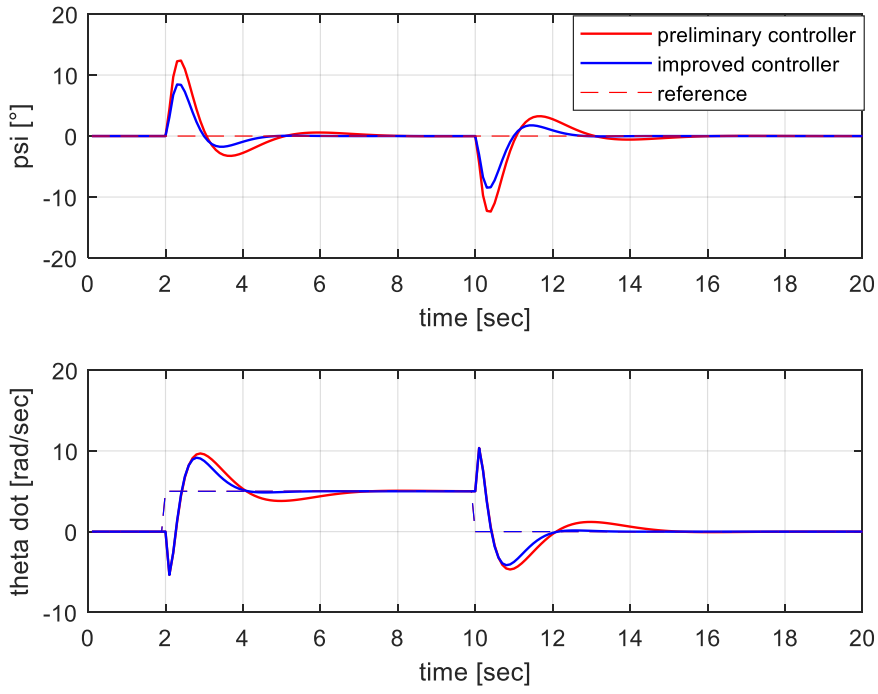

Figure 7.6 Body pitch angle (psi) and angular velocity of the sphere (theta dot) with a step input of 5rad/sec in velocity tracking for two controller models.

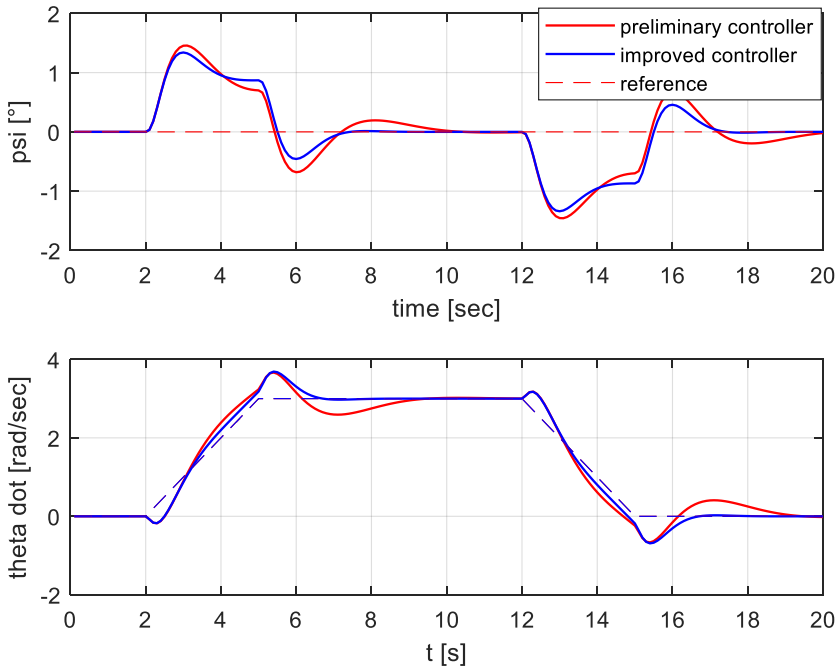

Figure 7.7 Body pitch angle (psi) and angular velocity of the sphere (theta dot) with a trapezoidal input in velocity tracking for two controller models.

It is noted as an improvement was achieved, observing a damping response for the new proposed system. It is also noted how better characteristically parameters (maximum overshoot and settling time) are obtained for both cases.

Chapter 8 - Conclusion

This thesis covered an early design phase for an innovative idea of mobile robot called Ballbot, the main objective was design and validate a model-based concept of this device.

As a first step, a physical model was developed starting with a simplified model of a two-dimensional decoupled system, later this model was improved by the introduction friction and the presence of a sloped surface. To finish the mathematical modeling, a linearized three-dimensional model was introduced, concluding that the two-dimensional model may be adopted under the hypothesis of small variations in pitch and roll angle.

In chapter 5 an optimal control theory was introduced for the implementation of an LQR (linear–quadratic regulator) controller to meet the system stability and achieve a velocity tracking given as input.

In chapter 6, the influence of the fundamental parameters as height and mass was analyzed, finding a strong impact in the behavior of the system, moreover, the limitation in the COM (Center Of Mass) distance, a key parameter in the design, was individualized.

Finally, the work ends with simulations of different input requirements which may require some future applications of the Ballbot, in each case the response was studied, and a control optimization was proposed in order to improve the dynamical behavior.

References

[1] R. Hollis, "Ballbots," *Scientific American,* pp. 71-72, 2006.

[2] C. M. a. S. J. David Effa, "SCALED SEGWAY SYSTEM DESIGN," Mechanical and Mechatronics Department University of Waterloo, Waterloo, 2015.

[3] E. Zurich, "http://rezero.ethz.ch/," Autonomous Systems Lab, [Online]. Available: http://rezero.ethz.ch/.

[4] T. Lauwers, G. Kantor and R. Hollis, ""One is Enough!"," in *12th International Symposium on Robotics Research*, October 2005.

[5] U. Nagarajan, A. Mampetta, G. Kantor and R. Hollis, ""State Transition, Balancing, Station Keeping and Yaw Control for a Dynamically Stable Single Spherical Wheel Mobile Robot," in *IEEE International Conference on Robotics and Automation*, Kobe, Japan, May 2009.

[6] S. Doessegger, P. Fankhauser, C. Gwerder, J. Huessy, J. Kaeser, T. Kammermann, L. Limacher and M. Neunert, " "Rezero, Focus Project Report"," Autonomous Systems Lab, ETH Zurich, June 2010.

[7] T. Endo and Y. Nakamura, ""An Omnidirectional Vehicle on a Basketball"," in *12th International Conference on Advanced Robotics*, July 2005.

[8] J. &. U. S. &. C. B. FONG, "899: BALLBOT," University of Adelaide, 2009.

[9] Y. Yamamoto, NXT Ballbot Model-Based Design, CYBERNET SYSTEMS CO., LTD, April 2009.

[10] B. P. Giovanni Jacazio, Meccanica applicata alle macchine, Torino: Libreria editrice universitaria Levrotto & Bella, 1991, 1991.

[11] M. &. B. L. Dalla Vedova, "Dry Friction Discontinuous Computational Algorithms," *International Journal of Engineering and Innovative Technology,* vol. 3, pp. 1-8, 2014.

[12] D. Karnopp, "Computer simulation of stick-slip friction in mechanical dynamic

systems," *Journal of Dynamic Systems, Measurement, and Control,* vol. 107, no. 1, pp. 100-103, 1985.

[13] M. S. R. H. a. G. K. Bhaskar Vaidya, "Operation of the Ballbot on Slopes and with Center-of-Mass Offsets," in *IEEE International Conference on Robotics and Automation (ICRA)*, Seattle, Washington, 2015.

[14] P. Fankhauser and C. Gwerder, Modeling and Control of a Ballbot, Zurich: ETH Zurich Research Collection, 2010.

[15] H. &. S. R. Kwakernaak, Linear Optimal Control Systems, Wiley-Interscience, 1972.

[16] J. P. a. A. E.-N. G. Franklin, Feedback Control of Dynamic, Pearson, 2006.

Appendix A - Derivation of the equations of motion

We start from:

$$\frac{d}{dt}\left(\frac{\partial L}{\partial \dot{\theta}}\right) - \frac{\partial L}{\partial \theta} = F_\theta \qquad \text{(A1.1)}$$

$$\frac{d}{dt}\left(\frac{\partial L}{\partial \dot{\psi}}\right) - \frac{\partial L}{\partial \psi} = F_\psi \qquad \text{(A2.1)}$$

Deriving respect theta θ and psi $\dot{\psi}$:

$$\frac{\partial L}{\partial \theta} = \frac{\partial T_1}{\partial \theta} + \frac{\partial T_2}{\partial \theta} - \frac{\partial U}{\partial \theta} = 0$$

$$\frac{\partial L}{\partial \dot{\theta}} = \frac{\partial T_1}{\partial \dot{\theta}} + \frac{\partial T_2}{\partial \dot{\theta}} - \frac{\partial U}{\partial \dot{\theta}}$$

$$\frac{\partial T_1}{\partial \dot{\theta}} = \frac{\partial\left[\frac{1}{2}M_s\left(R_s\dot{\theta}\right)^2 + \frac{1}{2}M_b\left(\left(R_s\dot{\theta} + L\,\dot{\psi}\cos\psi\right)^2 + \left(L\,\dot{\psi}\sin\psi\right)^2\right)\right]}{\partial\dot{\theta}} = M_s{R_s}^2\dot{\theta} + M_b{R_s}^2\dot{\theta} + + R_s M_b L\,\dot{\psi}\cos\psi$$

$$\frac{\partial T_2}{\partial \dot{\theta}} = \frac{\partial\left[\frac{1}{2}J_s\dot{\theta}^2 + \frac{1}{2}J_\psi\dot{\psi}^2\right]}{\partial\dot{\theta}} = J_s\dot{\theta}$$

$$\frac{\partial U}{\partial \dot{\theta}} = 0$$

$$\boxed{\frac{\partial L}{\partial \dot{\theta}} = M_s{R_s}^2\dot{\theta} + M_b{R_s}^2\dot{\theta} + J_s\dot{\theta} + R_s M_b L\,\dot{\psi}\cos\psi}$$

$$\frac{\partial L}{\partial \psi} = \frac{\partial T_1}{\partial \psi} + \frac{\partial T_2}{\partial \psi} - \frac{\partial U}{\partial \psi}$$

$$\frac{\partial T_1}{\partial \psi} = \frac{\partial\left[\frac{1}{2}M_s(R_s\dot{\theta})^2 + \frac{1}{2}M_b((R_s\dot{\theta} + L\,\dot{\psi}\cos\psi)^2 + (L\,\dot{\psi}\sin\psi)^2)\right]}{\partial\psi} =$$

$$= -M_b L\,\dot{\psi}\sin\psi\left(R_s\dot{\theta} + L\,\dot{\psi}\cos\psi\right) + M_b L\,\dot{\psi}\cos\psi\left(L\,\dot{\psi}\sin\psi\right)$$

$$= -M_b L\,\dot{\psi}\sin\psi\, R_s\dot{\theta}$$

$$\frac{\partial T_2}{\partial \psi} = \frac{\partial\left[\frac{1}{2}J_s\dot{\theta}^2 + \frac{1}{2}J_\psi\dot{\psi}^2\right]}{\partial\psi} = 0$$

$$\frac{\partial U}{\partial \psi} = \frac{\partial[(M_s + M_b)gz_s + M_b gL\cos\psi]}{\partial \psi} = M_b gL\sin\psi$$

$$\boxed{\frac{\partial L}{\partial \psi} = -M_b L\,\dot{\psi}\sin\psi\, R_s\dot{\theta} + M_b gL\sin\psi}$$

$$\frac{\partial L}{\partial \dot{\psi}} = \frac{\partial T_1}{\partial \dot{\psi}} + \frac{\partial T_2}{\partial \dot{\psi}} - \frac{\partial U}{\partial \dot{\psi}}$$

$$\frac{\partial T_1}{\partial \dot{\psi}} = \frac{\partial\left[\frac{1}{2}M_s(R_s\dot{\theta})^2 + \frac{1}{2}M_b\left((R_s\dot{\theta} + L\,\dot{\psi}\cos\psi)^2 + (L\,\dot{\psi}\sin\psi)^2\right)\right]}{\partial \dot{\psi}}$$

$$= -M_b L\cos\psi\left(R_s\dot{\theta} + L\,\dot{\psi}\cos\psi\right) + M_b L\sin\psi\left(L\,\dot{\psi}\sin\psi\right)$$

$$= -M_b L\,R_s\dot{\theta}\cos\psi + M_b L^2\,\dot{\psi}(\cos\psi^2 + \sin\psi^2)$$

$$\frac{\partial T_2}{\partial \dot{\psi}} = \frac{\partial\left[\frac{1}{2}J_s\dot{\theta}^2 + \frac{1}{2}J_\psi\dot{\psi}^2\right]}{\partial \dot{\psi}} = J_\psi\dot{\psi}$$

$$\frac{\partial U}{\partial \dot{\psi}} = \frac{\partial[(M_s + M_b)gz_s + M_b gL\cos\psi]}{\partial \dot{\psi}} = 0$$

$$\boxed{\frac{\partial L}{\partial \dot{\psi}} == -M_b L\,R_s\dot{\theta}\cos\psi + M_b L^2}$$

Furthermore

$$\frac{d}{dt}\left(\frac{\partial L}{\partial \dot{\theta}}\right) = \frac{d}{dt}\left(\left[[M_s + M_b]{R_s}^2 + J_s\right]\dot{\theta} + R_s M_b\dot{L}\,\dot{\psi}\cos\psi\right)$$

$$\frac{d}{dt}\left(\frac{\partial L}{\partial \dot{\theta}}\right) = \left[[M_s + M_b]{R_s}^2 + J_s\right]\ddot{\theta} + [R_s M_b L\cos\psi]\ddot{\psi} - R_s M_b L\,\dot{\psi}^2\sin\psi$$

$$\frac{d}{dt}\left(\frac{\partial L}{\partial \dot{\psi}}\right) = \left[M_b L^2 + J_\psi\right]\ddot{\psi} + [M_b R_s L\cos\psi]\ddot{\theta} - \left[M_b R_s L\,\dot{\psi}\sin\psi\right]\dot{\theta}$$

Introducing these terms in (A1.1) and (A1.2) we arrive to:

$$\left[(M_b + M_s){R_s}^2 + J_s\right]\ddot{\theta} + [M_b L R_s\cos\psi]\ddot{\psi} - M_b L R_s\dot{\psi}^2\sin\psi = F_\theta \qquad (3.1)$$

$$[M_b L R_s\cos\psi]\ddot{\theta} + \left[M_b L^2 + J_\psi\right]\ddot{\psi} - M_b gL\sin\psi = F_\psi \qquad (3.2)$$